CHAPTER II

Literature Review

The present localization theory is established and developed from the Mohr's strength theory published in the year 1900. This original theory of stress analysis has given a fundamental and crucial knowledge to various disciplines of engineers particularly in civil engineering. Mohr's theory describes the stress at a point by using the graphical illustration of circle. The drawing of this stress circle provide a clear understanding of stress conditions at failure. To explain the stress failure criterion, Mohr used the example of cast iron which was tested to failure in compression (σ_c), in tension (σ_t) and in pure shear (τ_{ult}). He then drew the linear lines contacting the compression and tension circles. These lines are extensively called "Failure envelopes" as illustrates in Figure 2.1.

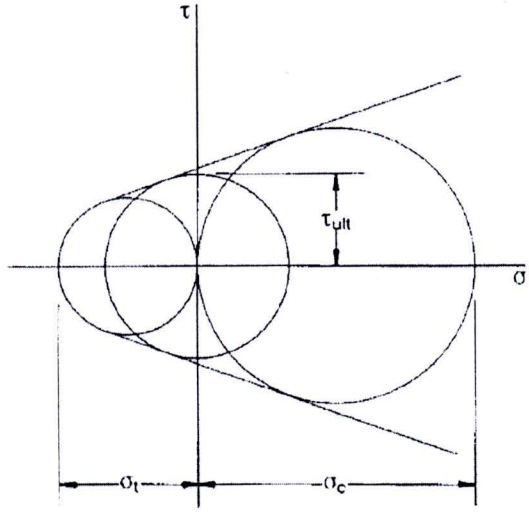

Figure 2.1 Mohr's stress circles and strength envelopes for cast iron (Parry, 1995)

Previously in 1773, Coulomb proposed various topics relating the strength properties of materials, i.e beams, earth pressure and shear strength of soils. A well-known equation concerning a shear resistance of soils was presented;

$$\tau_f = c + \sigma_n tan\phi \tag{2.1}$$

where τ_f is the shear strength per unit area; c is the soil cohesion; σ_n is the normal stress on the shear plane and ϕ is the shear resistance angle.

Although there are some differences of idea between Mohr and Coulomb failure criterion, however, the important conclusion is identical. Namely, both of original theories implied that the shear resistance of the materials will depend on its state of stress. This stress-dependent criterion is widely known as the "*Mohr – Coulomb failure criterion*". The stress analysis by the use of Mohr stress circle and the Mohr – Coulomb failure criterion can reveal an explicit view of stress conditions at failure in geotechnical engineering.

In the classical paper of Mohr in 1900, he finally summarized his findings by pointing to the following general property of localized deformation: " ... *The deformations observed in a homogeneous body after the elasticity limit [is reached] are not confined in the smallest domains of the body. They consist more or less in the fact that parts of the body of finite dimensions, displace with respect to each other on two sets of slip bands ...* " (Vardoulakis and Sulem, 1995).

2.1 Strain Localization in Granular Soils

In granular materials, when the applied load is high enough, the occurrence of strain localization will present. The inter-particle slip and rotation between particle surfaces will be generated which turn to strong dilatancy as well as high deformations of the material inside the localized zone. Because of the stability and deformation of the soil mass will be primarily influenced by the development of strain localization, therefore a research on strain localization problem in soils has been carried out in the field of geotechnical engineering for many years ago by theoretical, numerical as well as experimental works. As mentioned above, the basic concept of strain localization in sand has been evolved from a theoretical approach, i.e. Mohr - Coulomb criteria, then following by a numerical approach. In addition to the main developments of soil modeling in strain localization by theoretical and numerical approaches, various kinds of experimental studies have been attempted to clarify the crucial behaviors of strain

localization. These investigations have provided physical features, i.e. shear band orientation and thickness, as well as localization initiation time and evolution to the geotechnical engineers. Those research results also evidenced some influences of parameters affecting the nature of strain localization in sand, for example, an initial stress state, initial packing condition, grain characteristics of soil particle, specimen geometry and property of microstructure. The literature reviews of these investigations are as follows:

2.1.1 Theoretical and numerical approach

The theory of strain localization is an original work of Mohr to analyze strain localization in materials. It was applied to investigate the orientation of shear bands, i.e. inclination angle of shear band zone, within various types of materials, including elasto-plastic soils and rocks. A number of theories by many scholars have been proposed to make clear understanding about strain localization phenomena. Those theories can be liberalized as follows:

2.1.1.1 Theory of shear band inclination

Currently, There are two well-known theories in soil mechanics that can explain the physical property of strain localization, e.g. inclination of shear band. Those are Mohr - Coulomb theory and Roscoe theory.

- Mohr - Coulomb Theory

The Mohr - Coulomb theory, which is merely based on engineering static, can explicitly describe the orientation of the shear band in terms of inclination angle. This inclination angle of the shear band primarily depends on the mobilized frictional angle between grain particles. The Mohr - Coulomb theory states that the shear band plane of strain localization will parallel to the surface which passes through the failure stresses (σ_c, τ_c) on the Mohr - Coulomb failure envelope. The calculation of this classical theory can be displayed as in equation 2.2

$$\theta_c = \frac{\pi}{4} - \frac{\phi}{2} \tag{2.2}$$

where θ_c is the angle between the major principal stress direction and shear band, ϕ is the value of the mobilized friction angle at failure. By definition, the mobilized friction angle, ϕ, is calculated from the major and minor principle stress, σ_1 and σ_3

$$sin\phi = \frac{\sigma_1 - \sigma_3}{\sigma_1 + \sigma_3} \tag{2.3}$$

Figure 2.2 shows the inclination angle (θ_c) between the idealized plane of shear band and the plane of major principal stress. In should be noted that this concept excludes some parameters affecting strain localization mechanisms.

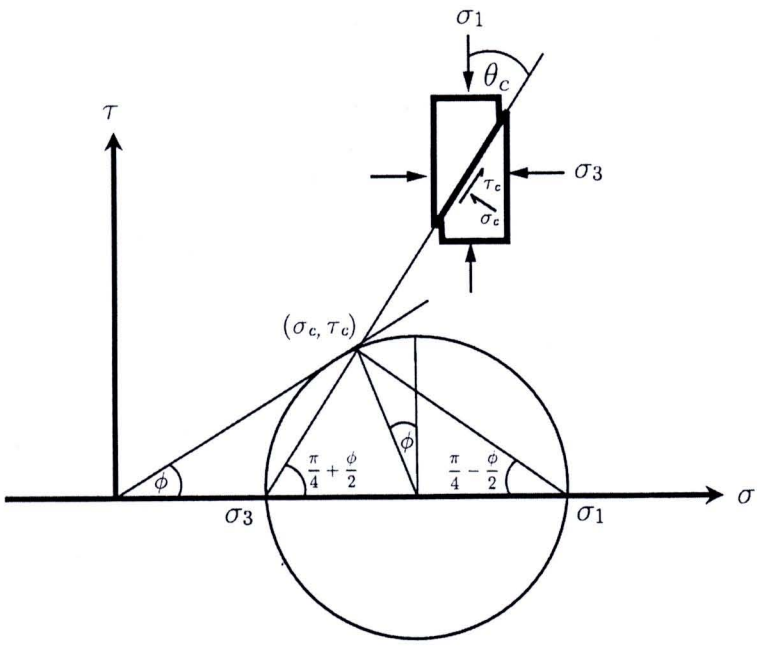

Figure 2.2 Mohr - Coulomb solution to shear orientation

- Roscoe Theory

Roscoe (1970), unlike Mohr's theory, proposed the strain circle on failure. He related the inclination angle of shear band with the angle of dilatancy as well as the major and minor principal strain increments. The expressions of these

correlations as well as the graphical explanation of Roscoe's finding can be displayed in equations 2.4, 2.5 and Fig. 2.3, respectively.

$$\theta_R = \frac{\pi}{4} - \frac{\psi}{2} \tag{2.4}$$

where θ_R is the inclination angle between the idealized shear band plane and the major principal strain increment direction, $d\varepsilon_1$, and ψ is the angle of dilatancy at failure. By definition, the dilatancy angle, ψ, is obtained from the major and minor principal strain increments $d\varepsilon_1$ and $d\varepsilon_3$:

$$sin\psi = -\frac{d\varepsilon_1 + d\varepsilon_3}{d\varepsilon_1 - d\varepsilon_3} \tag{2.5}$$

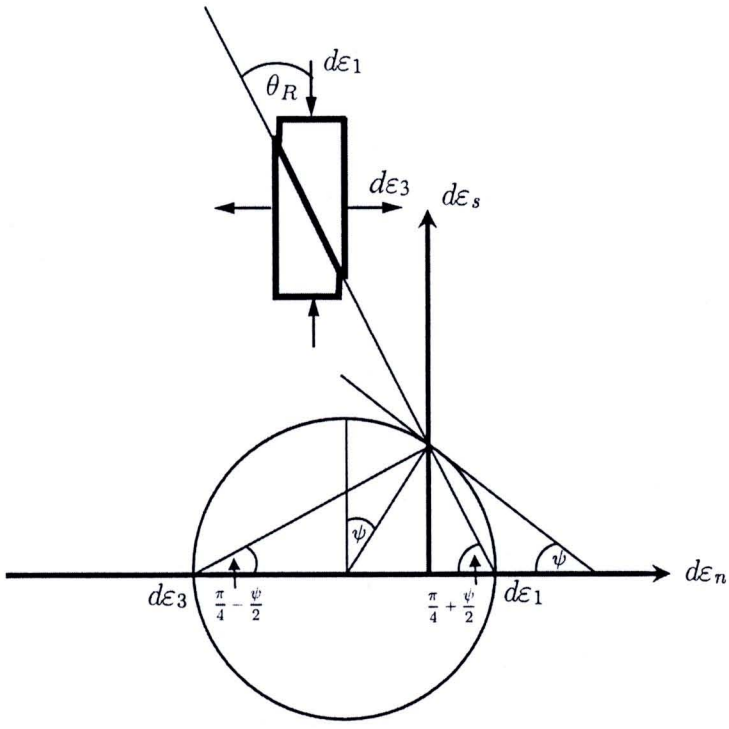

Figure 2.3 Roscoe solution to shear band orientation

- Arthur findings

Arthur *et al.* (1977) proposed the empirical equation concerning both parameters mentioned by Mohr and Roscoe, i.e. frictional angle and angle of dilatancy to comprehensibly explain the angle of inclination of shear band. His expression is as follows;

$$\theta_A = \frac{\pi}{4} - \frac{\phi}{4} - \frac{\psi}{4} \tag{2.6}$$

where θ_A is the inclination angle of the shear bands which include the effects of friction angle and angle of dilatancy. This equation was verified by theoretical and experimental study by Vermeer (1982) and Alshibli (1995), respectively.

Bardet (1990) compared experimental results of shear band inclination angle of various researchers, i.e. Arthur *et al.* (1977), Vardoulakis (1980) and Desrues *et al.* (1985), with the theoretical calculation of Mohr - Coulomb and Roscoe theory. He inferred that Mohr - Coulomb estimation underestimates the shear band orientation and this orientation does not vary in function of ψ as stipulated by the Roscoe theory. In contrast to the Mohr - Coulomb theory, Arthur's equation overestimates the shear band inclination angle. The use of the local dilatancy, ψ, established by Desrues *et al.* (1985) by using stereophotogrammetric technique, instead of the global dilatancy, ψ, slightly improves the prediction of shear band inclination angle. Finally he concluded that the theory of Arthur *et al.* (1977) and Mohr - Coulomb give an upper and lower bound value, respectively, for the shear band inclination angles which are more accurate than the prediction from the Roscoe theory. However, neither Mohr - Coulomb nor Arthur's equation accounts for the orientation of shear bands in all circumstances. It is therefore necessary to utilize a modern theory of strain localization to describe the emergence, orientation and mechanism of strain localization.

2.1.1.2 Theory of strain localization

- Theory of bifurcation

The theory of bifurcation has been established for more than 40 years ago in order to investigate the discontinuity inside the material body to study the behavior of strain localization in the post-bifurcation circumstance. The main idea of bifurcation theory is that the deformation inside the material will progress from a continuous mode to both continuous and discontinuous modes. When the localization initiates to present inside the mass body, the material will be divided into three main parts; the localization zone and two of intact zones. The mathematical concept of this bifurcation theory can properly describe the discontinuity inside the continuum. The unambiguous detail of these studies can be found in Vardoulakis (1979, 1983), Sulem and Vardoulakis (1990), and Vardoulakis and Sulem (1995). The bifurcation theory can be applied to the frictional and cohesive materials. It can be employed to simulate various modes of failure, i.e. necking, bulging, splitting and shear banding, inside the material. However, the failure mode of theory is yet influenced by many factors such as the loading conditions, boundary conditions as well as the constitutive model. As a result, a careful attention should be paid to avoid an undesired outcome from the analysis. It is also crucial to noted that this theory of bifurcation contains three important limitations: 1) it can only simulate the emergence of strain localization but cannot analyze its progression and development, 2) There is no warranty that during the analysis the strain localization will be manifested or not and 3) the determination of shear band thickness is not possible because of some limitations, i.e. no length scale, of continuum mechanic concepts.

- Cosserat continuum or Micropolar continumm

According to an ordinary continuum theory, the materials are ideally assumed as the continuum media. This assumption requires only translation degree of freedom of the particles. Therefore, this hypothesis is solely valid when the material response does not exhibit any discontinuity inside the body. It is widely recognized, however, that a non-homogeneous deformation inside the body will present after

reaching a peak state of stress. This discontinuity will take to an intense deformation within a finite zone of localization. Very high strain gradient variation followed by grain rotation, sliding and dilation will be observed within this zone. Due to the lacking ability of a conventional continuum and the complexity of strain localization, the Cosserat or Micropolar continuum can transcend those limitations by incorporating the rotational degree of freedom together with couple stresses in the analysis. The Cosserat theory can perfectly describe the grain rotation in addition to grain translation for the study of strain localization. Since the grain particles will rotate and translate when subjected to a substantial amount of pressure, for an analysis in the Cosserat continuum of a single grain, six degrees of freedom will be analyzed. The widely known studies of strain localization by using Cosserat continuum approach can be found in Kanatani (1979), Mühlhaus and Vardoulakis (1987), Vardoulakis and Sulem (1995) and Oda and Iwashita (1999).

- Strain gradient theory

Due to lack of some capacities of the conventional continuum mechanics to explain a complete behavior of strain localization, various researchers have proposed many new calculation techniques. One of these new approaches is the strain gradient theory. The advantages of this method are for example the capability to solve the mesh dependency in numerical simulation and the micro-scale of size effects. Aifantis (1984, 1987), Zbib and Aifantis (1988) included the length scale coefficient in their gradient plasticity model with shear band width to interpret size effects in metals. Vardoulakis and Aifantis (1989) used the second-order gradient theory in studying the heterogeneous deformation in the granular media. They had also modified a flow theory to incorporate high-order gradients and investigate the liquefaction problem in granular materials. During 1991, Vardoulakis and Aifantis had extended their works in 1989 to integrate the second-order gradients into the flow rule and the yield function, they were able to calculate the shear band thickness. Oka *et al.* (2001) used gradient dependent viscoplastic constitutive models to study the localizations in saturated soils. They had used the second-order strain gradient in the hardening function and found that strain localization is highly dependent on the strain

gradient. It may be implied that the results of strain localization simulation will be more accurate if strain gradient theory is combined with Micropolar theory in the analysis.

2.1.2 Experimental approach

Experimental studies of strain localization in granular materials have been performed by a series of researchers: Vardoulakis and co-workers (Vardoulakis *et al.*, 1978; Vardoulakis and Graf, 1985; Han and Vardoulakis, 1991), Tatsuoka and co-workers e.g. (Tatsuoka *et al.*, 1986; Tatsuoka *et al.*, 1990), Arthur (Arthur *et al.*, 1977; Arthur and Dunstan, 1982), Finno and co-workers (Finno *et al.*, 1996; Finno *et al.*, 1997), Desrues and co-workers (Desrues *et al.*, 1985; Desrues, 1990; Desrues *et al.*, 1996; Mokni and Desrues, 1999; Desrues and Viggiani, 2004). These researchers experimentally clarify many helpful answers relating to strain localization in geomaterials. The conclusions among them are as follows:

- Strain localization inside the geomaterials, i.e. sand, can be observed in the conventional and modern laboratory tests for example triaxial test, plane strain test, direct shear test and hollow cylindrical test

- The complex localization patterns might be the result of size and slenderness ratio of the specimens as well as loading conditions. In a short specimen, when test in a compression triaxial device, the complex pattern of shear band zones might be emerged due to the effect of boundary condition. However, those intricate shear bands will be vanished in a long specimen.

- At peak stress in stress-strain curve, many researchers, using various detection techniques, reported full establishment of strain localization or shear band zones. Plane strain experiments on sand performed by Desrues *et al.* 2004, using stereophotogrammetry to detect graphically the onset of strain localization, showed that the initiation time of strain localization is always observed at or before the peak stress-strain curve.

Besides the conventional tests in geotechnical engineering, i.e. plane strain and triaxial tests, various experimental techniques have been performed to help in studying the emergence and evolution of strain localization. Those techniques can quantify shear band volumetric, capture density variations quantitatively within shear band, measure physical characteristics, i.e. inclination angle and thickness, within shear band. The complete review of those testing methods are detailed in the following sections.

2.1.2.1 Plane strain test

Plane strain test or biaxial test is an ordinary test in geotechnical engineering to simulate the in-situ cases of soil behavior, i.e. strip footing and slope stability analysis. Several researchers, e.g. Lee (1970), Arthur *et al.* (1977), Vardoulakis (1977 and 1980), Vardoulakis *et al.* (1978), Peters *et al.* (1988), Finno *et al.* (1997), Desrues (1998) and Alshibli *et al.* (2003), have conducted the plane strain tests in many types of testing conditions to observe the localized deformation inside the soil sample. The higher peak value of stress followed by strain softening of stress-strain relation has been documented for sand of various packing conditions. The stress value also increases as the confining pressure increases. Moreover, the difference in a mode of failure between plane strain compression test and triaxial compression test can be evidently observed. The failure pattern of specimen in plane strain test is really uniform and distinct whereas in triaxial compression test the complex pattern of shear band can be detected. However, a unique and uniform width of shear band might be perceived in a long height of specimen under triaxial test. The emergence time of strain localization is also influenced by the condition of loading. Namely, strain localization under plane strain test occurs faster than that of triaxial test.

The experiment works of Vardoulakis (1977 and 1980) and Vardoulakis *et al.* (1978) at Karlsruhe University can show clearly an idea of plane strain compression test. In the apparatus shown in Fig. 2.4, wherein a sample 4×8×14 cm^3 was wrapped into a rubber mould of 0.3 mm thickness. A so-called Karlsruhe dry sand was used. The index properties of sand were: mean grain diameter d_{50} = 0.45 -

0.50 mm, grain size among 0.08 mm and 1.8 mm, uniformity coefficient U = 2, maximum specific weight $\gamma_d{}^{max}$ = 17.4 kN/m^3, minimum void ratio e_{min} = 0.53, minimum specific weight $\gamma_d{}^{min}$ =14.6 kN/m^3 and maximum void ratio e_{max} = 0.84. Two side plates used for the condition of plane strain; they carried polished stainless steel plate and a silicone grease to prevent boundary friction. The base and top plates were also polished and lubricated and carried 10 mm diameter porous stone to keep the sample in the center position. The base plate was placed on a movable roller bearing. In some tests, Fig. 2.4, the specimen did not include any artificial imperfection. In some other tests, Fig. 2.5, a small artificial initial imperfection (side notch or loose sand inclusion) was included. The test results showed that an internal shear zone was formed at the peak of the stress-strain curve. The thickness of the shear zone was about 3-5 mm, i.e., (10 - 15) × d_{50}, and the inclination angle of the shear zone was approximately 52 - 67°. This inclination angle was in accordance with the formula by Arthur *et al.* (1977). The shear zones were less steep in initially looser samples than in dense samples. The shape of the shear zone was influenced by the type of the imperfection (shear zones with a notch were slightly curved). Looser sands were more sensitive than dense ones. The maximum angle of internal friction decreased almost linearly with increasing void ratio.

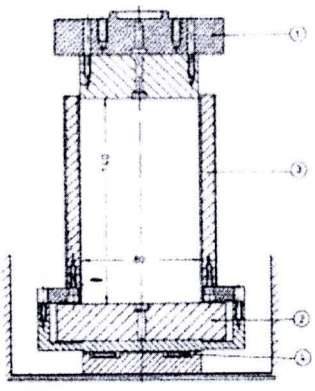

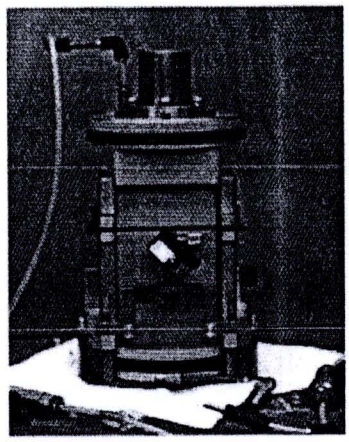

(a) (b)

Fig. 2.4 Plane strain compression apparatus: (a) System 1) top plate, 2) base plate, 3) side plates and 4) roller bearing, and (b) Photograph (Vardoulakis, 1977)

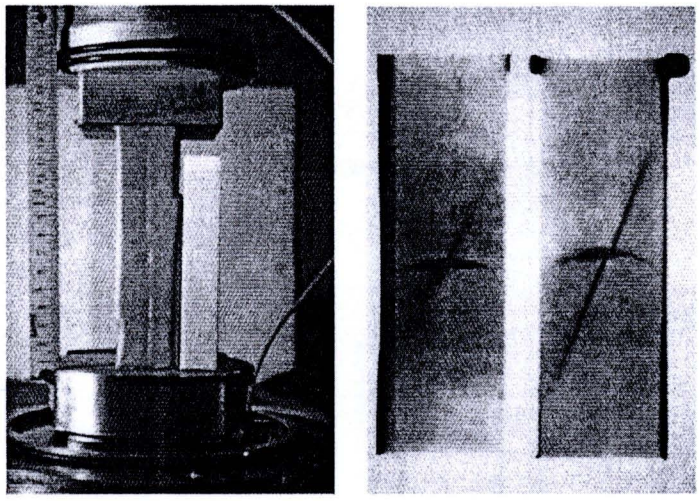

(a) (b)

Fig. 2.5 Formation of shear zone in dense specimen (a) without initial (b) with initial imperfection in the form of loose sand inclusion on the basis of X-rays radiographs (Vardoulakis, 1977)

Other well-known plane strain compression tests to study localization in sands are perform by Desrues (1985) and later modified by Hammad (1991) at Grenoble University. The Schematic diagram of a plane strain apparatus can be shown in Fig. 2.6. The results of their works showed that various patterns of shear zones were observed including even parallel and crossing shear zones depending on boundary conditions and slenderness of the specimen. The onset of shear localization took place slightly before the peak of the stress ratio. The inclination angle of shear zone decreased with increasing pressure. The shear zone thickness decreased as the confining stress and initial density increased. The reduction of the specimen size or its slenderness delayed the onset of strain localization. For higher slenderness ratio, other bifurcation modes, e.g. buckling, were more likely to occur. The shear zone thickness increased with increasing particle size and its inclination angle was not affected by the mean grain size and non-uniformity of sand grading. The inclusion of material imperfection dictated the location of the shear zone and acted as a trigger for the onset of shear localization.

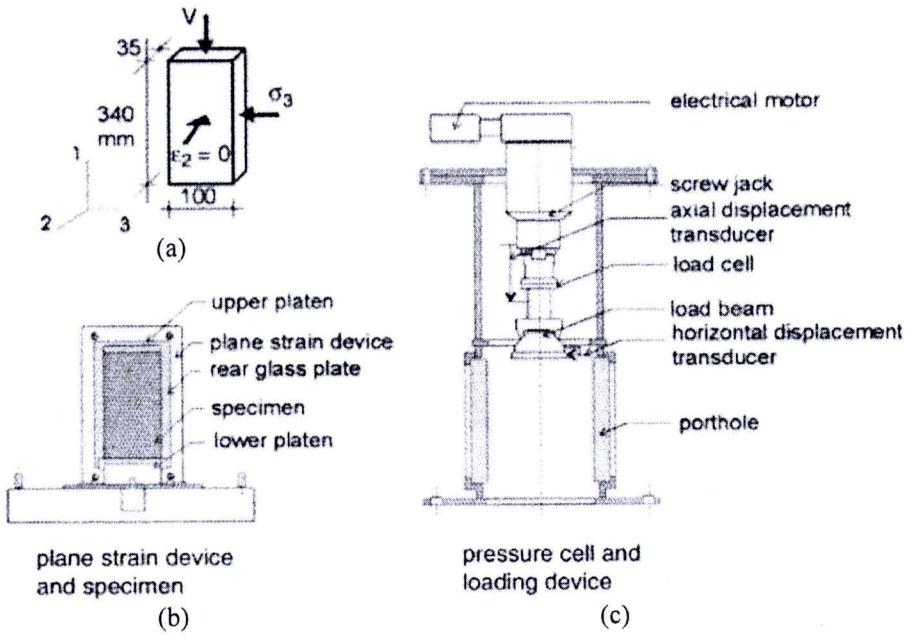

Fig. 2.6 Schematic diagram of a plane strain apparatus at the University of Grenoble: (a) specimen geometry, (b) plane strain device and specimen, (c) pressure cell and loading device (Desrues and Viggiani, 2004)

2.1.2.2 Triaxial test

Two types of conventional triaxial test, i.e. triaxial extension and triaxial compression test, have been performed continuously since 1970 to investigate the behavior of strain localization within soil samples in laboratory. Roscoe *et al.* (1963) demonstrated that the conventional triaxial extension test has substantially more problems associated with strain localization than the triaxial compression test. Yamamuro and Lade (1995) investigated the behavior of granular materials in triaxial extension test both drained and undrained test of cylindrical specimens to study the influence of plastic strain localization in granular materials. They found that the failure was rapidly occurred in all conventional extension tests and the strain localization appeared to begin very early during the shearing process. They also concluded that the conventional extension test is inherently unstable and exhibits the high scattered testing results. The axisymmetric conventional triaxial compression test, CTC, is the most common experiment used by geotechnical engineers to observe the strength and deformation responses of soils. However, in the CTC experiments

localization patterns are more difficult to detect and describe. In CTC, there are two modes of failure that can be occurred, localized shear plane mode or bulging diffuse mode, depending on the density and geometry of the specimen and the confining pressure. Alshibli *et al.* (2003) indicated that the confining pressure and specimen packing condition have a profound influence on the behavior of CTC specimens. Specimens show a very high-peak friction angle followed by severe softening for specimens tested under very low-confining pressures and the amount of softening decreases as the confining pressure increases. All CTC specimens show nearly the same residual stress regardless of the confining pressure value.

Desrues *et al.* (1996) performed the axisymmetric CTC tests. The diameter of the sand specimen was 100 mm and the height was 100 or 200 mm. A special anti-friction system was used. The shear zones were detected using X-ray tomography. The tests were carried out on dense and loose sand with lubricated and non-lubricated specimens. In initially dense specimens, localization of deformation was observed to depend greatly on test conditions. In a dense specimen with non-lubricated ends, the slightly curved shear zone was created (Fig. 2.7). When the specimen was short, the localized deformation was initiated with a single rigid cone attached only to one of the platens but the other platen did not generate any cone (Fig. 2.8).

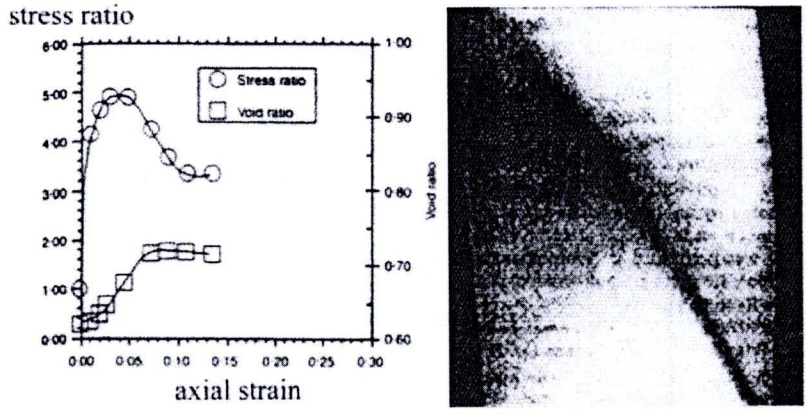

(a) (b)

Fig. 2.7 (a) Evolution of the stress ratio and void ratio (b) formation of a shear zone during the experiment with a high dense specimen and non-lubricated ends (Desrues *et al.*, 1996)

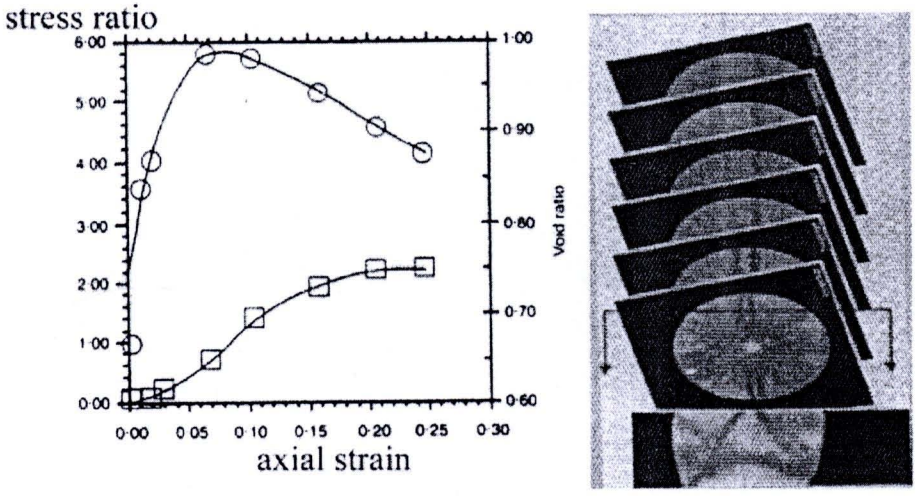

(a) (b)

Fig. 2.8 (a) Evolution of the stress ratio and void ratio (b) formation of shear zones during the experiment with a low dense specimen and lubricated ends (Desrues *et al.*, 1996)

2.1.2.3 X-ray imaging techniques

The visual investigations of strain localization mechanisms have been carried out over the years. These techniques are for example X-ray radiography, Computerized Tomography and Digital Image Analysis (DIA). Roscoe (1970) performed experimental studies on plane strain models of different geotechnical structures such as retaining walls. He used an X-ray technique to measure the displacement of small lead shot distributed in the sand mass. He could observe the dark bands on the radiographs, then stated that, "*this dark band represents the rupture surface in which the sand has dilated to the critical state*". The same observation was made using the same X-ray technique by other researchers in triaxial test, plane strain biaxial test, simple shear apparatus, and directional shear cell. Though, these X-ray measurements have given most valuable qualitative information on localization patterns in sand specimens, but they generally contain three limitations: the lack of quantitative data on the observed density changes, the limitation to plane strain

experiments, and the lack of providing the 3-D radiograph or images. Fig. 2.9 shows the result of the X-ray photography acquired from plane strain test.

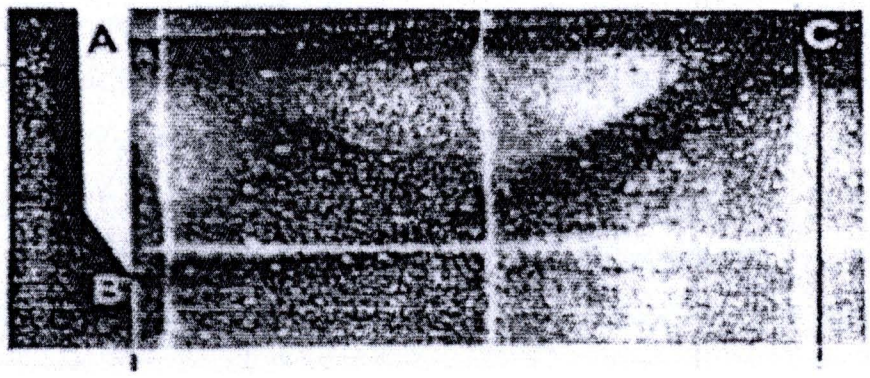

Fig. 2.9 X-ray photography used on plane strain models allowed Roscoe and his collaborators to show the large dilatancy taking place in shear zones in the modeling of retaining wall (Roscoe *et al.*, 1970)

2.1.2.4 Stereophotogrammetric method

Stereophotogrammetry, firstly applied to soil mechanics experiments by Butterfield *et al.* (1970), provides the measurement of local volumetric strain increment in sand. This method had been further developed and extensively used by many scholars, i.e. Vardoulakis (1979, 1980) in Karlsruhe and Desrues *et al.* (1985). Desrues and Viggiani (2004) explained in their paper that the advantage of this technique was an ability to capture non-homogeneous strain throughout the test. The method of "False Relief Stereophotogrammetry" (*FRS*) is based on the analysis of photographs taken from a fixed viewpoint at different times during the loading process. An essential feature of *FRS* is that the deformation can be directly perceived as a fictitious relief by using the well-known stereoscopic effect on successive pairs of photographs. In the application of *FRS* to observe strain localization of sand, the difference of deformation between successive images will be calculated and recorded. When these two photographs are viewed in stereo, displaced regions appear elevated, with the elevation proportional to the magnitude of displacement. In the presence of a shear band, the deforming specimen appears as two planes of different elevation connected by a slope. For a given pair of photographs and thus a given increment of the global axial strain, the shear band can be therefore completely characterized, in

terms of both width and orientation. These systematic analysis of successive photographs of the deformed specimen allowed for observing the evolution of localized deformations throughout the test. The use of stereophotogrammetry as a quantitative tool can use to present the evolution of localized deformation in terms of incremental strain fields. Fig. 2.10 shows the stereophotogrammetry-based incremental fields of shear strain intensity and volumetric strain. Although digital image correlation software nowadays becomes a competitive method to study strain localization. This numerical image correlation is easier to use and requires less efforts in the analysis. However stereophotogrammetry has some benefits especially when strong discontinuities present in the body.

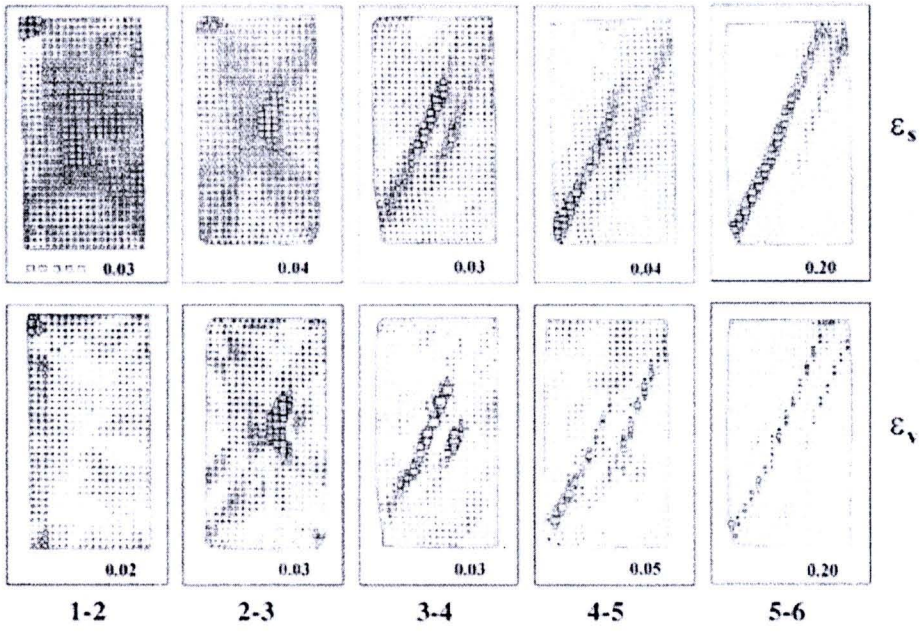

Fig. 2.10 Stereophotogrammetry-based incremental fields of shear strain intensity (top row) and volumetric strain (bottom row)
(Desrues, 1985)

2.1.2.5 Gammametry techniques

Gammametry technique is used for local density measurements. This conventional technique has been used by several authors for many years. In the studies of strain localization, this technique was used in Grenoble by Desrues (1984), and Desrues *et al.* (1985) to perform quantitative measurements of mass density

changes in the localized shear zones of sand specimens subjected to plane strain loading (Fig. 2.11).

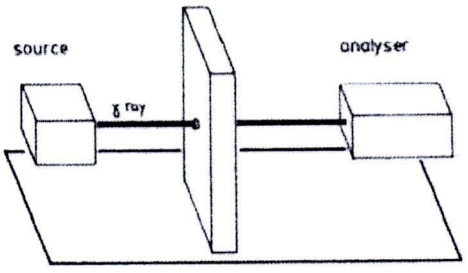

Fig. 2.11 Gamma-ray device used to measure the local density in shear bands in plane strain specimens (Desrues, 1984)

The studies by Desrues was performed on both plane strain and true triaxial tests. In both cases, the specimens was loaded to failure then unloaded and kept to a constant volume by applying a vacuum pressure to the specimen. This temporarily hardened sample was then transferred to a Gamma-ray device in order to measure the density profile within the shear band zone. The intensity of the attenuated beam was measured by a detector. In both cases, significant dilation can be captured in the shear band zones. Fig. 2.12 and 2.13 show the density profile across a shear band and density profile before and after loading in plane strain test of dense specimen with low confining pressure, respectively.

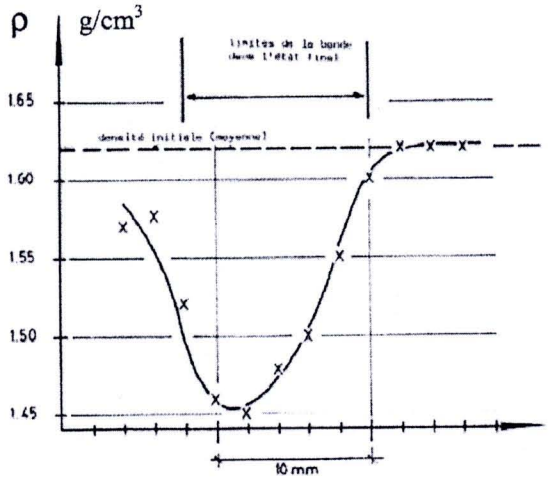

Fig. 2.12 Density profile across a shear band in plane strain test of dense specimen with low confining pressure recorded by Gamma-ray absorption (Desrues, 1984)

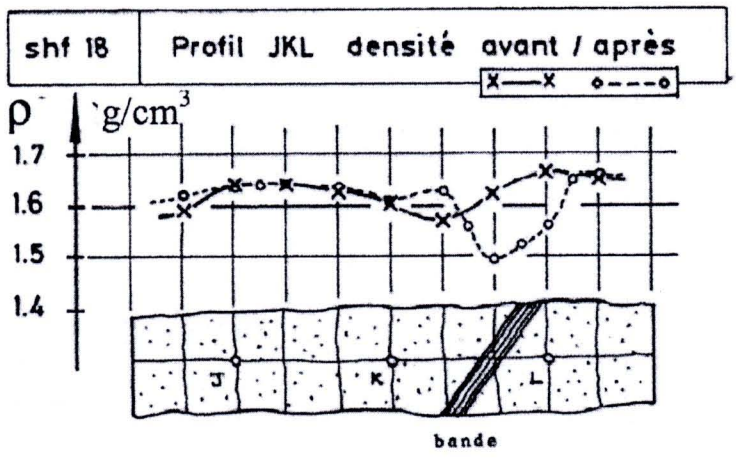

Fig. 2.13 Density profile before and after loading in plane strain test of dense specimen with low confining pressure (Desrues, 1984)

2.1.2.6 Computerized Tomography (CT)

Computerized Tomography (CT) has been extensively used in the medical inspection throughout the human body by medical practitioners. The common name is known as "X-ray scanner". This technique can be used to measure the density variation within the specimens. A three-dimensional figure can also be displayed by combining the adjacent slices of two-dimensional density map acquired from several angles across a single plane. The sample of experimental setup of CT system device can be illustrated in Fig. 2.14 by Desrues *et al.* (1996).

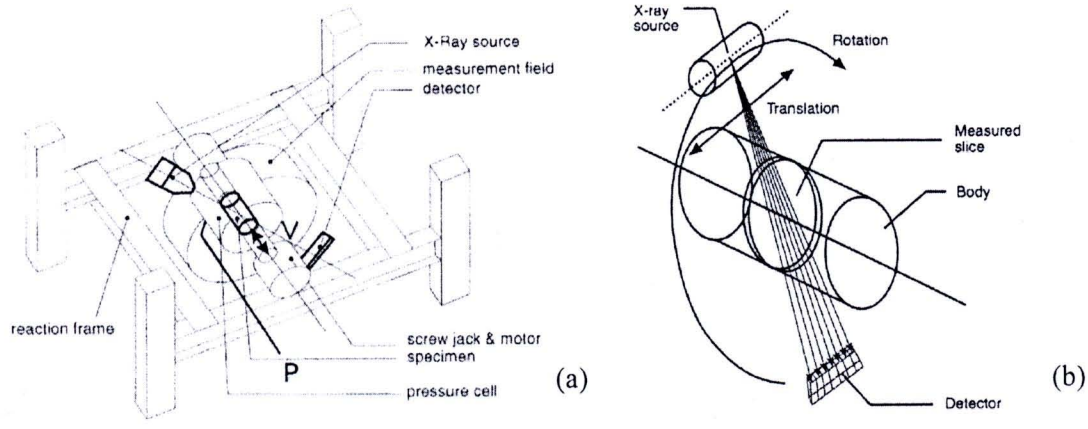

Fig. 2.14 (a) Experimental device: specimen, triaxial cell, scanner field measurement and reaction frame (b) the technique of CT scan (Desrues *et al.*, 1996)

The uses of CT technique to study the strain localization in geotechnical engineering can be found in the literature. Raynaud *et al.* (1989) and Vinegard *et al.* (1991) had published their works of axisymmetric triaxial tests and showed that CT technique could describe some important characteristics of strain localization, i.e. density variations, inside rock specimens. Hicher *et al.* (1994) used CT to study strain localization in clay specimens. Their studies showed the density alteration inside the localized zone. Namely, the density in the shear band zone was increased relating to the rest of the specimen. However, in undrained tests, no density change could be observed within the shear band zone, though direct visualization confirmed the emergence of strain localization in these tests. For the granular materials, CT technique is extensively used to acquire a series of images of shear band as well as the evolution of strain localization from both of plane strain and triaxial compression test by Desrues (1984), Desrues *et al.* (1996), Alshibli *et al.* (2000 and 2003), and Batiste *et al.* (2004). Their results reveal that the inception and the development of the localization in sand specimens could be well detected and described, both qualitatively and quantitatively. Fig. 2.15 shows the images of CT scan technique of two orthogonal axial sections and two cross sections taken at one third and two thirds of the specimens height under conventional triaxial compression experiments with various test conditions (Alshibli *et al.*, 2003).

2.1.2.7 Digital Image Analysis (DIA)

Most of the experimental studies on strain localization were dependent on the visual observations of deformation profile within the specimens. Because of a rapid revolution of computer industry both in software and hardware development. Digital Image Analysis (DIA), to some extent, allows the researchers to capture and analyze local strain within the specimen as a function of global strain for the strain localization analysis. During the loading process, DIA was used to monitor the entire specimen uniformity, initiation time of localization as well as to determine the specimen dimensions.

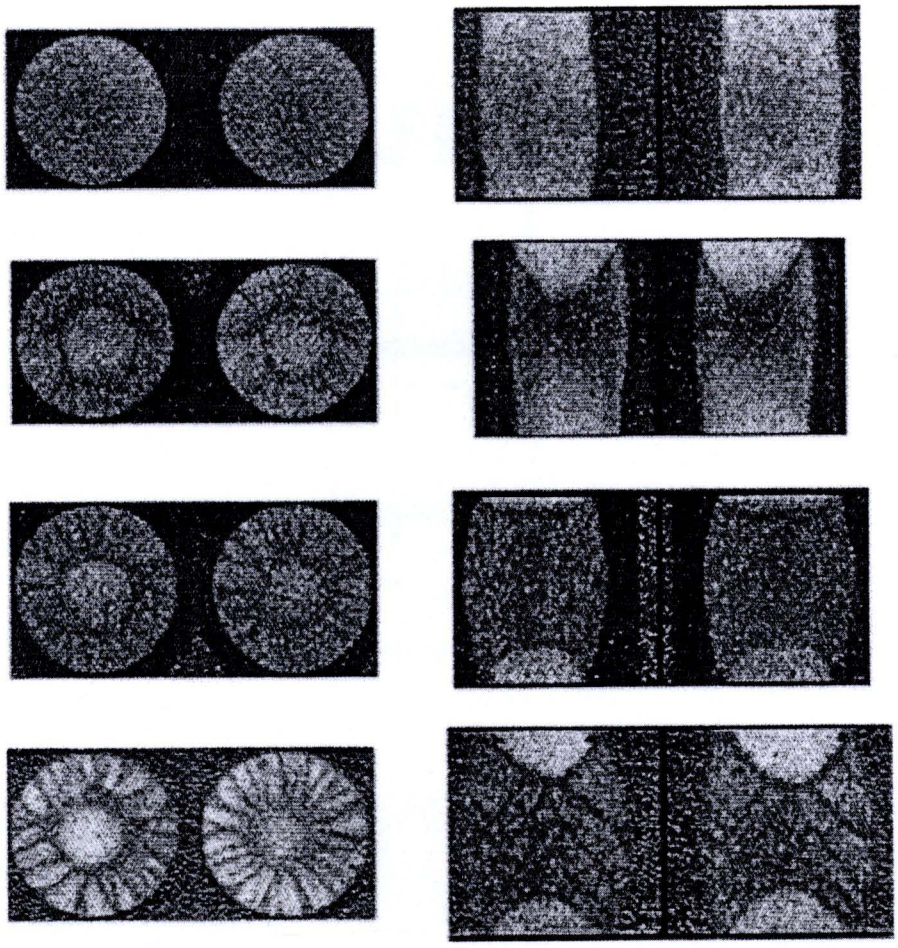

Fig. 2.15 shows CT scan technique of two orthogonal axial sections and two cross sections taken at one third and two thirds of the specimens height under conventional triaxial compression experiments with various test conditions (Alshibli *et al.*, 2003)

Alshibli and Sture (1999) used the DIA to study localized deformations in granular materials tested under plane strain condition (Fig 2.16). They used two independent DIA techniques to measure the shear band thickness. In the first technique, the digitized optical images of a grid printed on the latex membrane, known as a surface measurement, were used to measure the shear band orientation angle and thickness (Fig. 2.17). The second technique used an ultra-low viscosity resin to harden the specimen in preparation of epoxy impregnation and thin-sectioning to study microscopic images of the internal fabric (Fig. 2.18). The observation of this microscopic images is a quantitative analysis of local void ratio of sand. Void ratios are calculated based on the relative areas occupied by voids and particles within these slices.

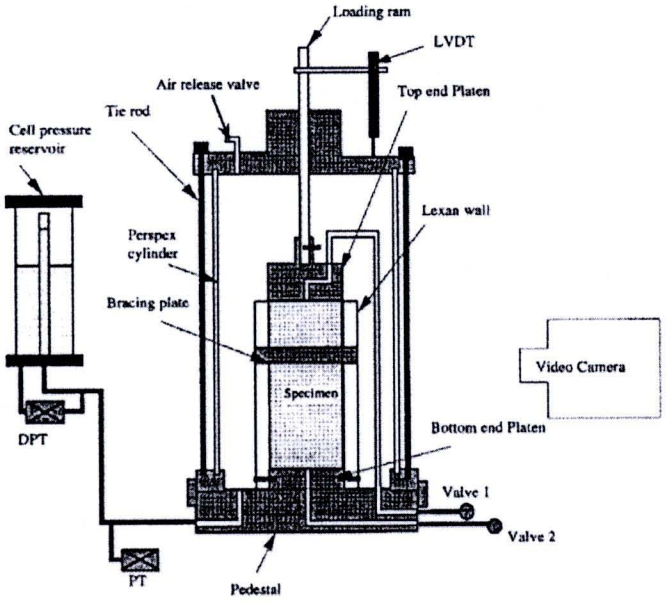

Fig. 2.16 Schematic of experiment apparatus to study strain localization by DIA (Alshibli and Sture, 1999)

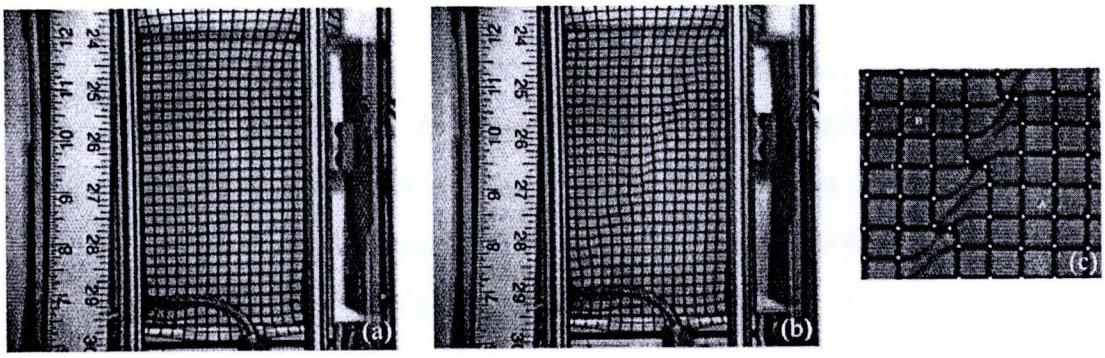

Fig. 2.17 Specimen image (a) before compression (axial strain = 0 %) (b) deformed specimen at 3.8% axial strain (c) magnified image showing grid relative displacement within shear band (Alshibli and Sture, 1999)

Alshibli and Sture (1999) finally concluded that DIA demonstrates an excellent ability in accurately measuring localized deformations in granular materials. Localized deformations of granular materials can be easily and accurately monitored and measured using surface digitization. Moreover, they summarized that microscopic image measurements, from epoxy impregnation and thin-sectioning, of the void ratio variation can be accurately used to measure the shear band thickness. Shear band thickness measurements obtained from membrane surface digitization and epoxy impregnation techniques are also very close.

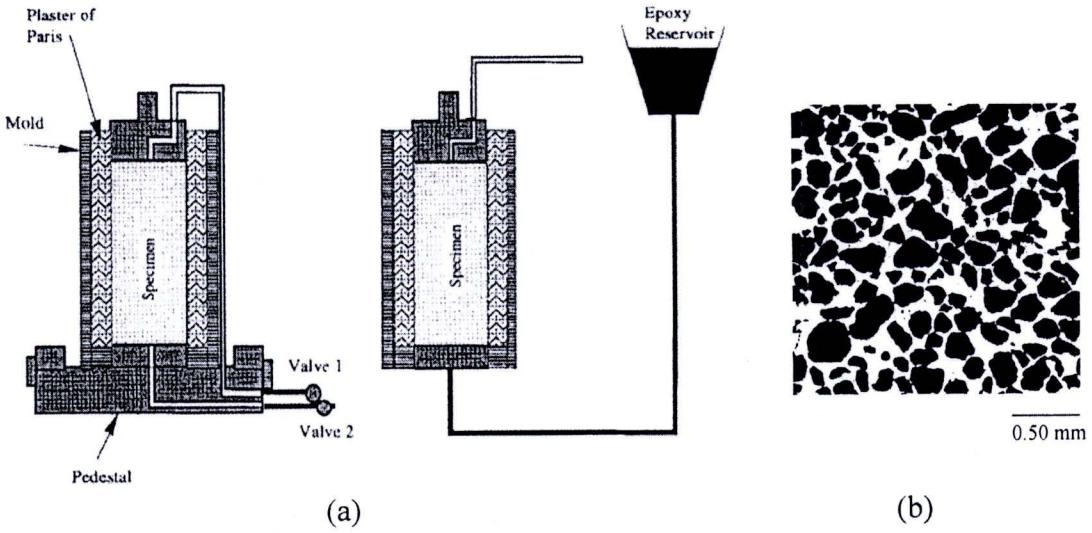

Fig.2.18 (a) Schematic of cross section of specimen resin impregnation setup (b) typical microscopic image of the tested sand after hardening in the epoxy (Alshibli and Sture, 1999)

Sachan and Penumadu (2007) used DIA to evaluate the strain localization mechanisms, i.e. evolution of shear bands with respect to the loading boundary conditions, in the solid cylindrical Kaolin clay specimens sheared by using lubricated end both in compression and extension triaxial tests. A latex membrane, thickness of 0.3 mm with dots marked in a grid pattern, was placed on the cylindrical specimen used for triaxial testing, which was confined in a cast-acrylic cylinder filled with water. The dots on the membrane were tracked using high resolution digital images taken by a 2.1 million pixel resolution (1792 H: 1200V) of digital camera. This digital camera was placed at about 562 mm distance from the outer wall of cell and mounted on a two-axis controller, which allowed for precisely adjusting camera position in two directions. A soft light was also used to provide uniform illumination of the triaxial specimens and significantly reduced shadows in the digital images. Fig. 2.19 shows the digital image setup and prepared Kaolin clay specimen for triaxial test. After finishing an experimental work, all captured images will then be downloaded to a personal computer to measure the coordinates of the dots by image analysis software. After processing the images taken during triaxial test and developing the contour plots to illustrate the strain field, they found that corresponding local strain contour plots indicated the formation of strong localized deformation zones at high

strain levels. As a result, these contour plots could present the evidence of the occurrence of strain localization due to shear banding within the clay specimen. Moreover, the variation in strain localization patterns of soil specimen could also be used to evaluate the influence of confining stress, loading conditions, stress history, drainage conditions, and soil's microfabric in lubricated-end triaxial tests (Fig. 2.20).

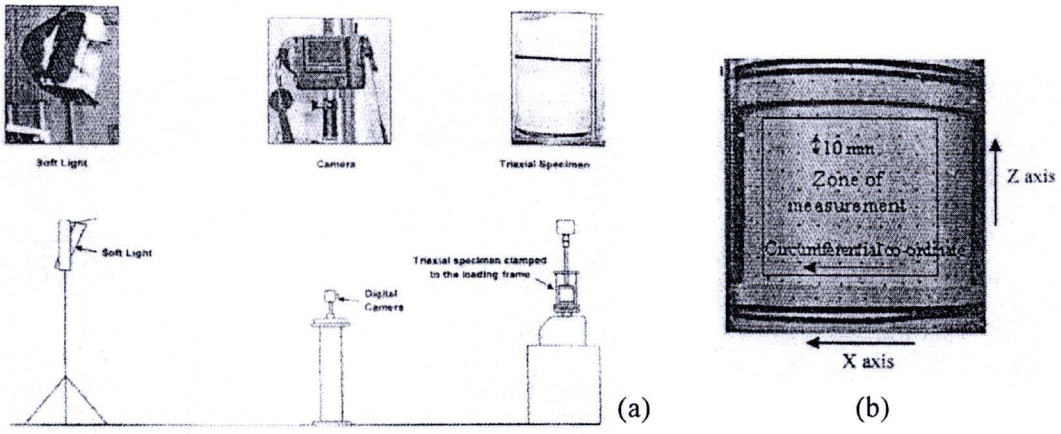

Fig. 2.19 Strain localization using DIA techniques (a) digital image setup (b) prepared Kaolin clay specimen (Sachan and Penumadu, 2007)

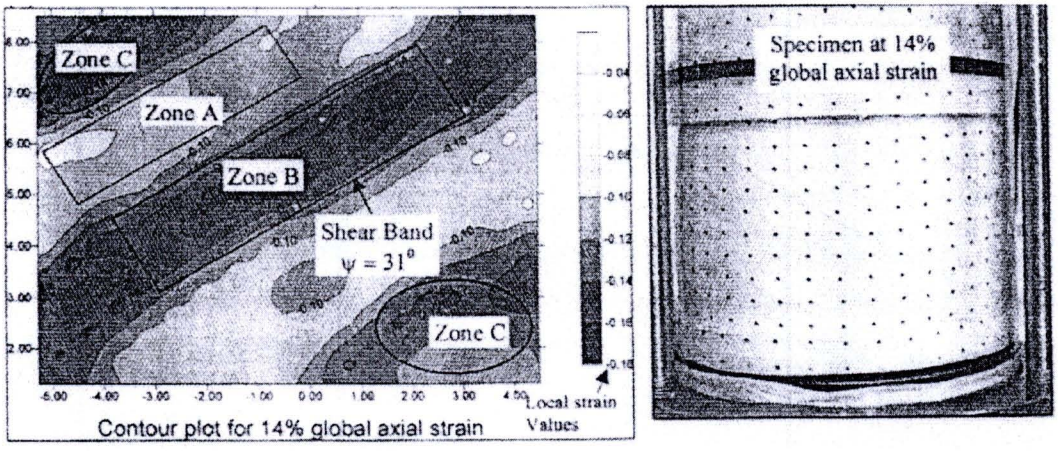

Fig 2.20 An example of contour plots and the digital image of shear band formation (Sachan and Penumadu, 2007)

2.1.2.8 Digital Image Correlation (DIC)

The basic concept of Digital Image Correlation (DIC) is the correlation of a group of points or pixels between two digital consecutive images taken at

different times in a deformation process. By overlapping these groups of pixels, a complete field displacement can be obtained and identified in the computer software. Rechenmacher and Finno (2004) had performed the plane strain compression experiments on dense sands by the technique of DIC to quantify directly internal strain field. They found that the use of DIC technique is a highly accurate technique for quantifying localized displacements in sands. Fig. 2.21 illustrates the images of displacement fields from DIC techniques.

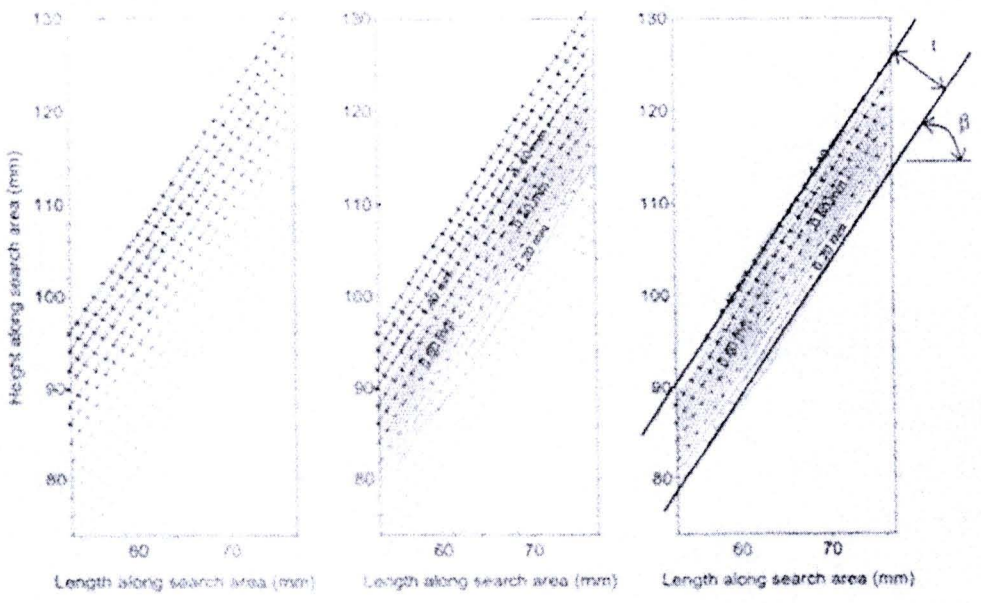

Fig. 2.21 DIC measured displacements surrounding a persistent shear band
(a) DIC displacements (b) contour fitted to displacements (c) shear band displacement points isolated for strain localization (Rechenmacher and Finno, 2004)

2.2 Factor Affecting Strain Localization

There are a number of factors that influence the physical mechanisms of strain localization or shear band, i.e. thickness, orientation as well as the initiation time of strain localization. These factors include the initial stress state, confining stress, grain characteristics and the geometry of the specimen. The influences of these factors will be further discussed in the following sections.

2.2.1 Mean effective stress and confining stress

Desrues *et al.* (1989) performed the testing program to find the dependency of shear band on mean stress level and density in sand. Tests on water-saturated RF Hostun sand were conducted on both dense and loose specimens with initial packing conditions of approximately 95% and 25%, respectively. The initial mean stress applied to the dense sand varied from 100 - 800 kPa with the specimen slenderness of 3.35 for all tests. The results are shown, in Fig. 2.22 and 2.23, in terms of stress ratio t/s' and volumetric strain, ε_v, as a function of axial strain ε_1. Stereophotogrammetry indicated that for all four tests, shear banding initiates at, or shortly before, a point of peak stress ratio and the subsequent stress ratio drop is associated with the complete development of a single shear band. The influence of initial mean stress on the conditions for the onset of shear banding is obvious from stress-strain responses from dense RF Hostun sand (Fig. 2.22). The higher the confining effective stress, the later the strain localization occurs. Also the peak value of t/s' clearly depends on the confining stress, namely it increases with decreasing of confining pressure. In conclusion it can be stated that for a given density of sample, an increase in the initial mean stress delays the appearance of strain localization.

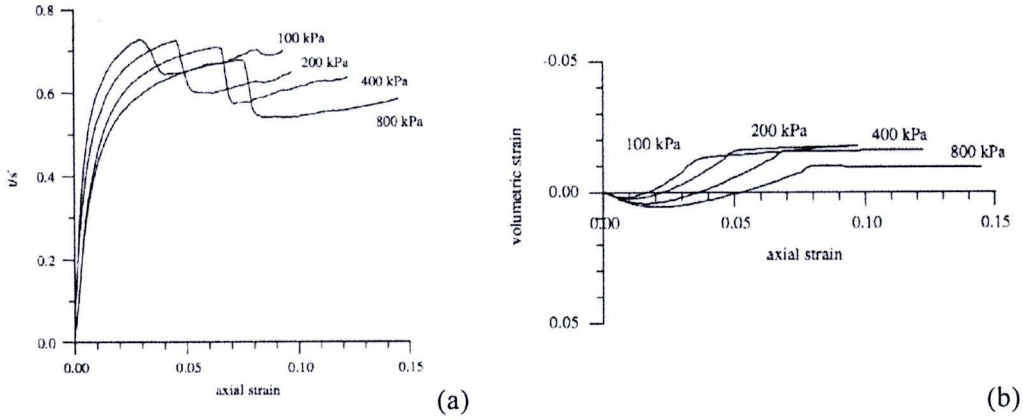

Fig. 2.22 Stress strain responses from four tests on dense RF Hostun sand:
(a) stress ratio (b) global volumetric strain versus global axial strain (Desrues, 2004)

Fig. 2.23 shows the results from four tests on loose RF Hostun sand in the same range of initial mean stress as for the dense specimens. The specimen slenderness was kept constantly at 3.35 for all tests. In these tests, the curve of the

effective stress ratio and axial strain does not exhibit any sharp peak, which is typical for loose specimens. Moreover, the increase in the confining pressure also delays the onset of strain localization as on the dense specimens.

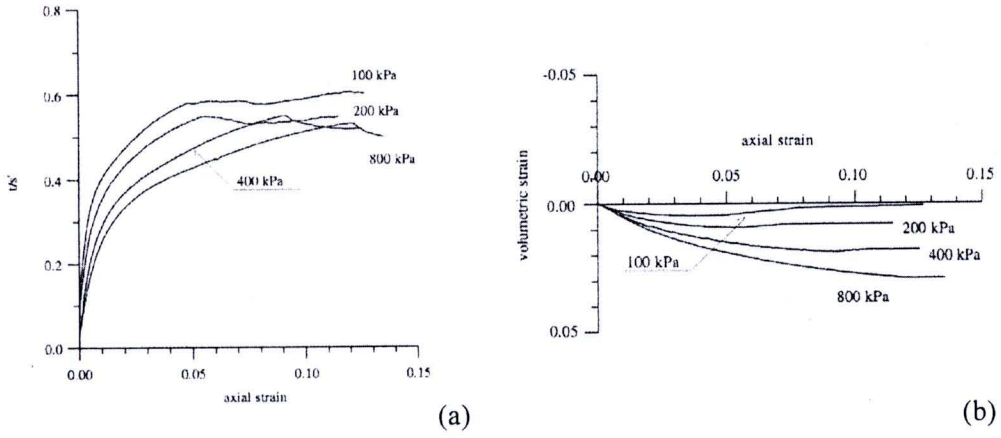

Fig. 2.23 Stress strain responses from four tests on loose RF Hostun sand: (a) stress ratio; and (b) global volumetric strain versus global axial strain (Desrues, 2004)

Desrues (2004) also reported that the shear band thickness depends on both initial density and mean effective stress, as first suggested by Tatsuoka *et al.* (1986). He stated that for a given sand the width of the shear band decreases as the confining stress and the initial density increase. For dense Hostun sand, shear band thickness reduces from 22 to $13 d_{50}$ as the effective confining stress increases from 100 to 800 kPa. A similar trend is observed for loose Hostun sand, the range of measured shear band widths being 31 to $17 d_{50}$ over the same range of confining stress.

Alshibli *et al.* (2003) investigated the effects of confining pressure on strength properties and localization phenomenon in sands. A uniform subrounded to rounded natural silica sand known as F-75 Ottawa sand was used in their investigation. A series of conventional triaxial compression (CTC) experiments were tested under very low-confining pressures, 0.05 - 1.30 kPa, in addition to the results of normal to high confining stress, i.e. 10 - 70 kPa, to investigate the effect of confining pressure on the constitutive behavior of sands. Fig. 2.24 illustrates the outcome of some tests. They concluded that the confining pressure have a profound influence on the behavior of CTC specimens. Specimens show a very high-peak friction angle and dilatancy angles

followed by severe softening for specimens tested under very low-confining pressures and the amount of softening decreases as the confining pressure increases. Both angles decrease as the confining pressure increases. All CTC specimens show nearly the same residual stress regardless of the confining pressure value.

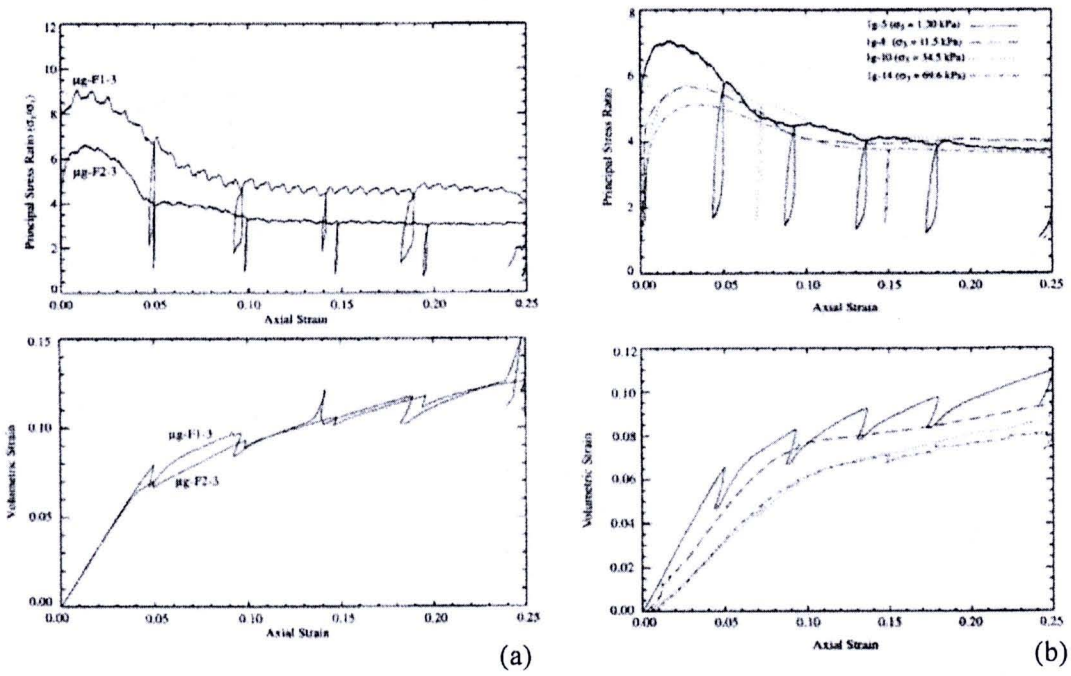

Fig. 2.24 Principal stress ratio versus axial strain and volumetric strain versus axial strain for CTC (a) confining pressure = 1.30 kPa (b) confining pressure = 1 - 70 kPa (Alshibli *et al.*, 2003)

2.2.2 Loading conditions

It is widely known that the stress-strain behavior and failure pattern of granular materials under plane strain (PS) test are different from the conventional triaxial compression (CTC) test. The failure of plane strain specimens always occurs along a unique and uniform shear plane. In the axisymmetric triaxial tests either localized shear plane or bulging diffuse failure modes occur depending on the density of the specimen and the confining pressure. Lee (1970) performed a series of drained and undrained PS and CTC experiments on fully saturated fine-grained sand. The results revealed that PS specimens reach higher values of maximum principal stress ratio than do CTC specimens, and the difference decreases as void ratio increases.

Moreover, PS specimens fail at smaller axial strain with a severe softening compared to CTC specimens. He finally concluded that the difference between PS and CTC results is greatest for dense specimens tested under low-confining pressure and that the difference decreases as confining pressure increases. Marachi *et al.* (1981) also performed a series of PS and CTC experiments on sand. Specimens were prepared to various initial void ratios. All experiments were performed under drained and air-dry conditions. Fig. 2.25 shows a comparison of the stress-strain relationship for both cases. The results are very similar to the behavior reported by Lee (1970).

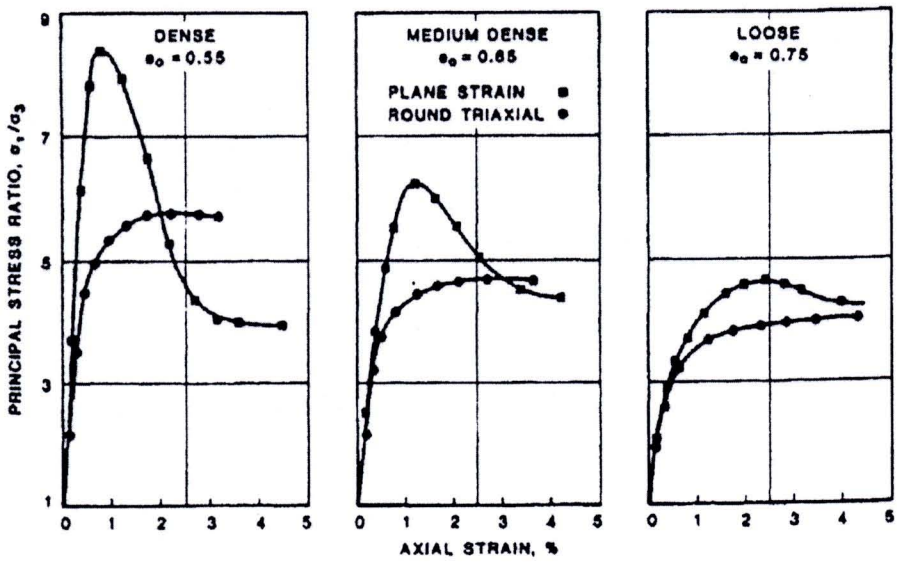

Fig. 2.25 Stress-strain relationship for plane strain and triaxial specimens (Marachi *et al.* 1981)

Fig. 2.26 shows the results of experimental investigation between CTC and PS tests under low and high confining pressure of silica sand performed by Alshibli *et al.* (2003). PS specimens showed higher-peak stress value followed by severe softening. In all cases, the CTC experiments show very similar principal stress ratio versus axial strain responses. A very small strain softening can also be observed after the peak stress value and the specimens reached the residual stress condition at about 10% axial strain. They also concluded that the failure of specimens subjected to PS loading condition is characterized by distinct shear bands accompanied by softening in the stress response depending on the specimen density and confining pressure. In contrast, the specimens in CTC experiments bulge uniformly in the vicinity of peak

stress and develop complex multiple symmetrical radial shear bands at higher axial strain levels. Therefore, It is quite clear from those results that the deformation processes and the stability behavior are quite different between triaxial and plane strain tests.

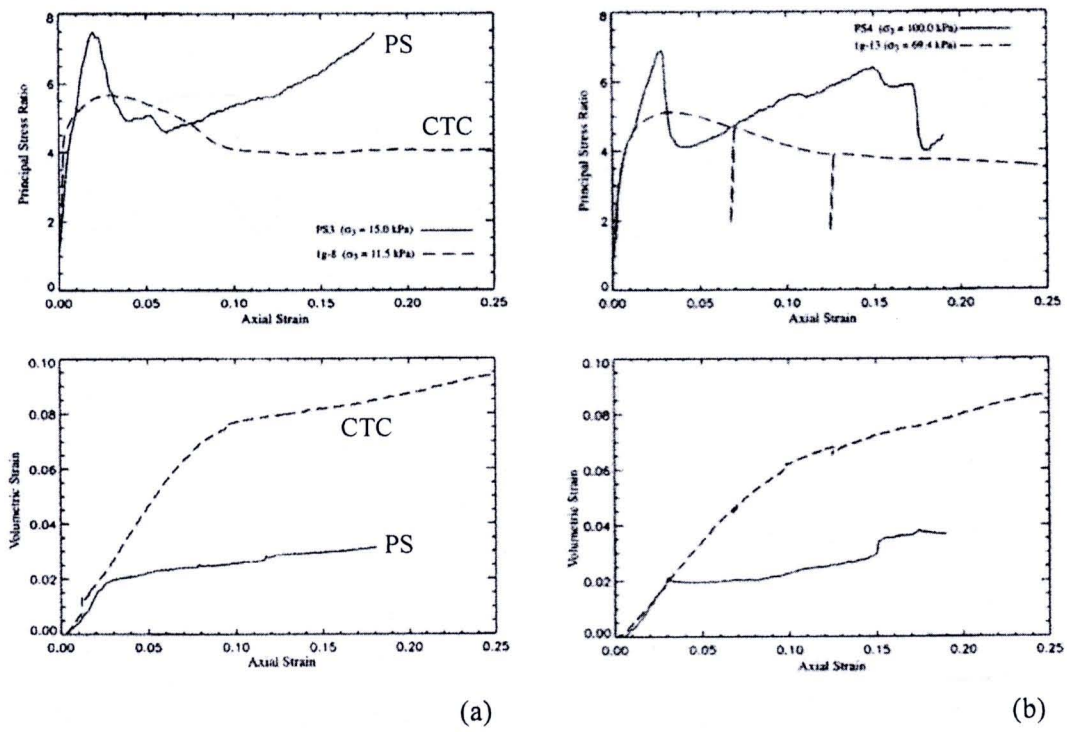

Fig. 2.26 Comparison between CTC and PS experiments of dense specimens tested under (a) low confining pressures and (b) high confining pressures (Alshibli *et al.* 2003)

2.2.3 Specimen geometry

Desrues *et al.* (1996) studied strain localization in triaxial tests on sand to observe void ratio evolution inside shear bands by using computed tomography (CT). Two of their tests performed with long specimens (slenderness ratio = 1.94 and 1.90). The result showed that a long specimen exhibits a single shear plane, though not perfectly planar, at a global axial strain (ε_a =7%) and remained the unique localization structure for larger strain (Fig. 2.27). In contrast to the above rather simple localization pattern, a short specimen (Slenderness ratio = 1.00) gave more complex localization pattern. Namely, a rigid cone, attached to the end platen, can be observed. This cone is delimited by a circular shear surface which is the locus of a large

dilatancy (Fig. 2.28). Moreover, the onset of localization was significantly delayed in the short specimen comparing to the relatively long specimen.

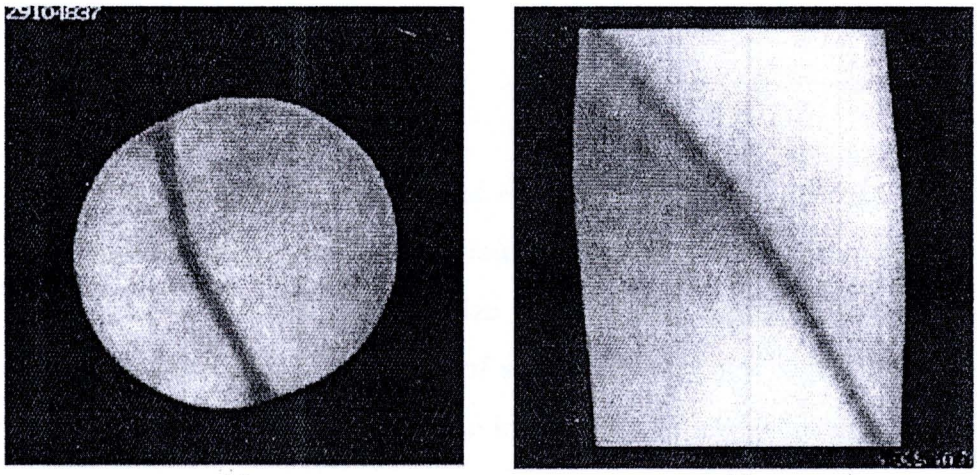

(a) (b)

Fig. 2.27 Trace of the single shear plane in long specimen of Triaxial test on sand (a) in a section perpendicular to the axis (b) containing the axis of the specimen (Desrues *et al.* 1996)

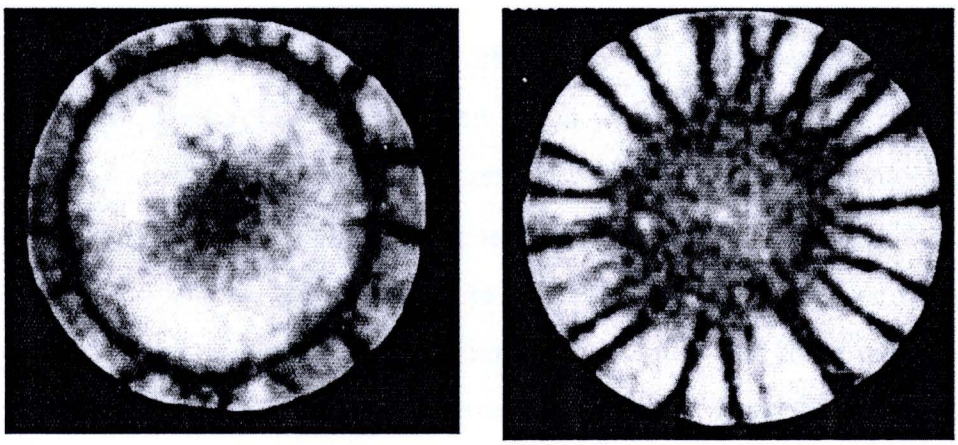

(a) (b)

Fig. 2.28 Two cross-sections recorded in a short specimen, revealing complex localization patterns (a) near the upper platen (b) at the middle height of the specimen (Desrues *et al.* 1996)

The effect of specimen geometry can also be observed in a paper carried out by Desrues (2004). He performed a number of plane strain compression tests on both dense and loose RF Hostun sands by varying four different values for the specimen slenderness (0.5, 1, 2, and 3.3). Three main conclusions can be summarized as

follows: the reduction of specimen slenderness ratio has the effect of (i) retarding the onset of strain localization (ii) reducing the steepness of the shear band and (iii) increasing the thickness of shear band.

2.2.4 Grain size

There are substantial experimental evidences showing that strain localization in sand depends on microstructure, i.e. grain size of the particles. For a certain stress state and loading conditions, different size of sand grain exhibit different responses both in terms of orientation and width of shear bands as well as the strain level at which shear banding occurs. These behaviors cannot be only explained in terms of macroscopic aspects such as void ratio and stress state. Many parameters such as shape and angularity of grains and grain size distribution profoundly influence the strain localization mechanism. Viggiani *et al.* (2001) investigated the influence of grain size distribution on strain localization in sand. The tests performed under different gradations of the same sand in terms of both the mean grain size and uniformity. Saturated specimens of the different sands were tested in plane strain under drained conditions starting from high relative densities. False relief stereophotogrammetry was used to capture the onset of strain localization and for accurately measuring the width and orientation of shear bands. The results confirm the dependence of the shear band thickness on the mean grain size (d_{50}). The testing results indicate that the ratio between shear band thickness and the mean grain size tends toward a constant limit value of approximately 7 for the largest grain size.

2.2.5 Role of imperfection

Desrues *et al.* (1996) and Desrues (2004) had investigated the influence of material imperfection on the behavior of strain localization by placing an artificial inclusion, i.e. a cylindrical of paper, cotton sphere and compact wood with a rough surface, into the sand specimen during sand deposition in the mold. The results showed that the location of the shear band is dictated by the location of the inclusion (Fig. 2.29) but the global stress–strain responses do not show any major deviation from the responses obtained from all the other tests performed at the same confining

pressures and initial density but without any inclusion. The plots of incremental strain field also reveals that in many cases strain localization initiates at more than one locations within a specimen. As the deformation progresses, a process of competition occurs among these different localization structures, with only one well-defined structure eventually taking over the others. On the contrary, in an imperfect specimen strain localization goes immediately to its final structure. This is a remarkable effect of the imperfection. Desrues, however, reported that the nucleation point for the initiation of localization in an imperfect specimen would not be occurred if an inclusion was placed in an axisymmetric position, i.e. on the axis at mid-height, inside the specimen (Fig. 2.30). This means that, in order to act as a localization attractor, an imperfection has not only to be strong but also it has to break the symmetry of the specimen.

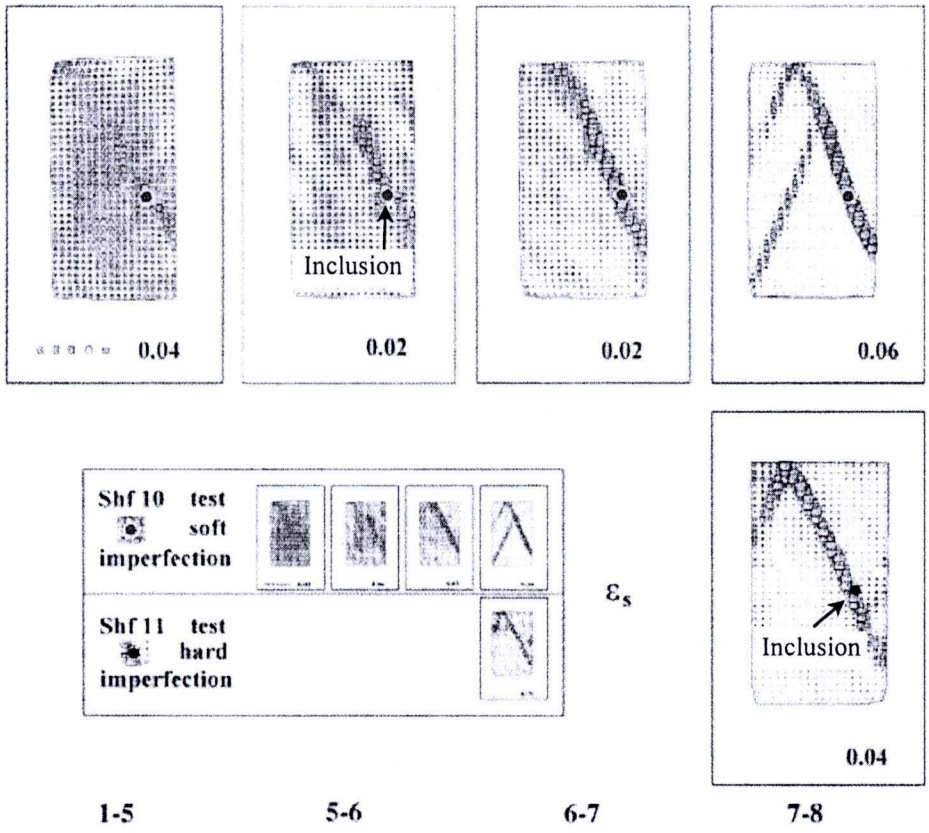

Fig. 2.29 Stereophotogrammetry-based incremental fields of shear strain intensity for soft (top row) and hard (bottom row) imperfection. (Desrues, 2004)

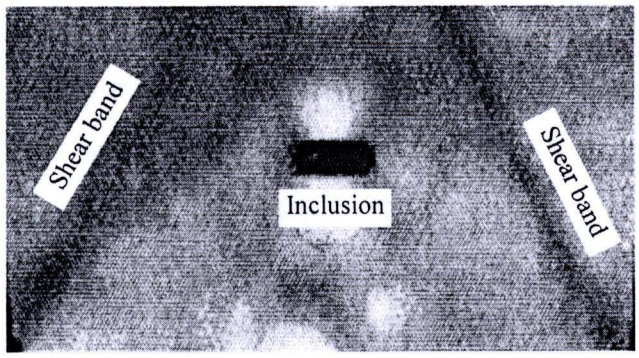

Fig. 2.30 Reconstruction of void ratio field in an axial tomogram of sand specimen: dark disc in the middle of the picture is a soft imperfection placed on the axis of the specimen; localization zones did not pass through the imperfection (Desrues *et al.* 1996)

2.3 Bender Element Test and Shear Wave Velocity in Particulate Materials

2.3.1 Bender element

The original concept of bender element application for geotechnical engineering was the work of Lawrence (1963 and 1965) who used piezoelectric crystals to generate one dimensional compression waves through sand and glass beads. Then, Shirley (1978) was the first to use piezoceramic bender element for generating and receiving shear waves in laboratory tests. Generally, bender element consists of two sheets of piezoelectric ceramic material such as lead, zirconate titanate, barium titanate, or lead titanate sandwiching a center shim of brass, stainless steel, or other ferrous nickel alloys to add strength to it (Fig. 2.31a). When a electrical voltage is applied to the bender element, the polarization will cause a bending displacement and, thus, the bender element acts as a signal generator. When the element is forced to bend, a voltage is generated and, thus, the bender element can act as a signal receiver. If one end is anchored, the other end generates a shear wave, or *S-wave* in the longitudinal direction of the crystal and compression or primary waves, *P-wave*, on the sides (Fig. 2.31b).

Over the years, bender elements have broadly employed in a number of geotechnical testing apparatuses. Bates (1989), Brignoli *et al.* (1996), and Pennington *et al.* (2001) measured shear wave velocity in triaxial specimens using peizoceramic

bender elements. Dyvik and Madshus (1985) measured small strain stiffness, G_{max}, of soil specimens in resonant column, odometer, and direct simple shear apparatuses using bender elements. Kawaguchi *et al.* (2001) measured G_{max}, in an odometer using bender elements. Agarwal and Ishibashi (1991) used bender elements in a triaxial cubical box device.

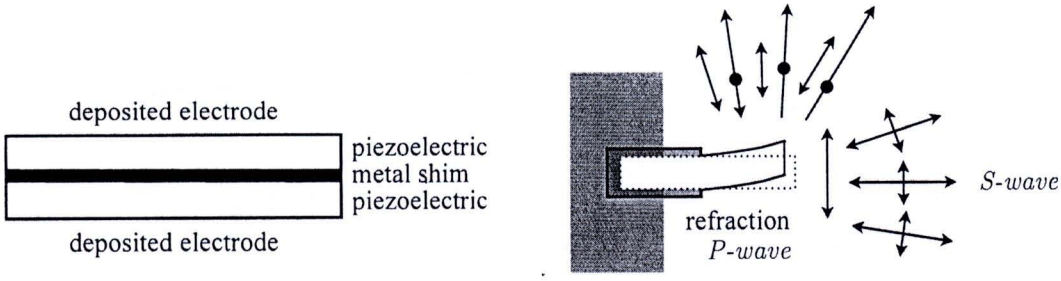

Fig 2.31 Bender elements (a) schematic representation of a bender element (b) directivity: both *P*- and *S-waves* are generated (Lee and Santamarina, 2005)

Among the different types of piezoelectric ceramics, lead zirconate titanate (PZT) is the most common used. Depending on polarization, there are two types of bender element: x-poled and y-poled. From the energy point of view, there is no difference between x-poled and y-poled. Both the x-poled and y-poled bender elements act similarly when connected in a series connection and a parallel connection, respectively. The bender element types and connections can be illustrated in Fig. 2.32.

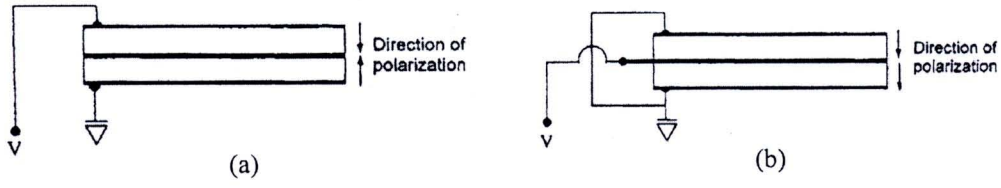

Fig. 2.32 Bender element types and connections (a) x-poled with series connection (b) y-poled with parallel connection (Lee and Santamarina, 2005)

In the bender element test for shear wave velocity measurement, a pair of peizoceramic of bender elements is used. One of the elements acts as the shear wave

transmitter and the other elements acts as the receiver. A schematic diagram of the bender element system is shown in Fig. 2.33. By measuring the travel time of the wave, the shear wave velocity, V_s, is determined as follows:

$$V_s = \frac{L}{t} \tag{2.7}$$

where L is the tip-to-tip distance between transmitter and receiver of bender element and t is the travel time of the shear wave from transmitter to receiver (Fig. 2.34). Since L can be easily measured by a dial gauge attaching in the apparatus, the error in the shear wave velocity calculation is mainly due to an inaccuracy of travel time determination and interpretation.

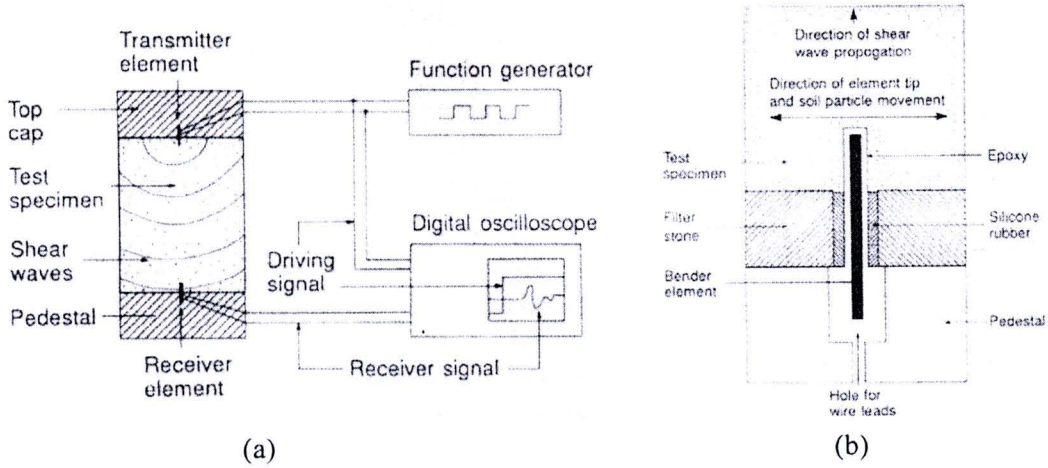

Fig. 2.33 Schematic of bender element system (a) setup of test equipment (b) detail of bender element connection to soil sample (Piezoceramic bender element test data sheet of Norwegian Geotechnical Institute, NGI)

2.3.2 Travel time determination

Based on a number of previous works, it is generally accepted that the travel distance is the distance between the tip of two bender elements. However, there is considerable uncertainty regarding the determination of travel time. Various waveforms, such as sine and square waves, with various frequencies, have been recommended as an excitation signal. Also, various methods have been studied for

determining the travel time such as time of flight techniques, i.e. first arrival time, the travel time between the characteristic points, and a cross-correlation method, and phase-sensitive detection technique. The details of each method can be explained in the following sections.

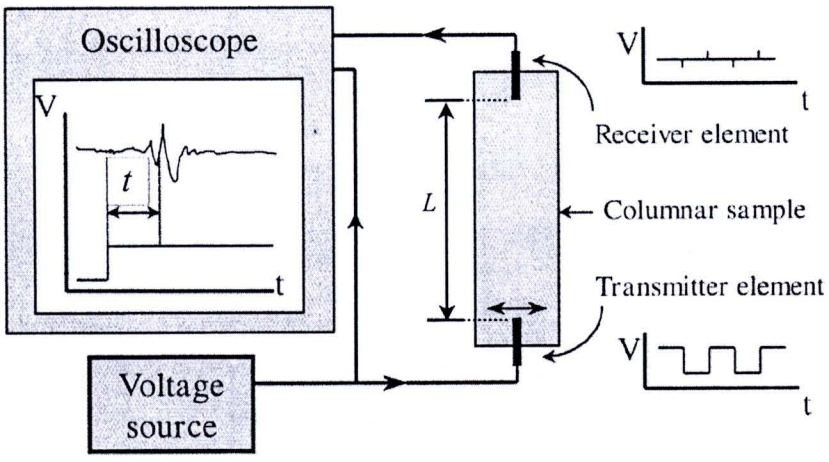

Fig. 2.34 Schematic representation of the conventional travel time measurement for shear wave velocity calculation (Blewett *et al.* 1999)

2.3.2.1 Time of flight techniques

The time of flight techniques use a single pulse as the transmitting signal. Initially, single square excitations have been used as seen in Fig. 2.35a. Many authors have then reported the difficulty in identifying the exact time of arrival signal. Thus Viggiani and Atkinson (1995) suggested the use of a single-shot sinusoidal excitation pulse, shown in Fig. 2.35b, to identify the points of similarity between the input and output waveform. Three different methods of travel time interpretations were generally used in order to find the times of travel from source to receiver. A detailed description of these three methods is provided below.

- First time of arrival

Kumar and Madhusudhan (2010) described that the first time of arrival, t_0, is the different time between the source signal and the receiver signal. In the case of the *S-wave* measurement, the initial weak signal for the receiver was found to be present in all the cases as indicated in Fig. 2.36a; this weak signal indicates the

presence of the near field effect. On the other hand, in the case of the *P-wave* measurements, the arrival of the receiver wave was quite distinct and there was no presence of any initial weak signal at all; see for instance Fig. 2.36b.

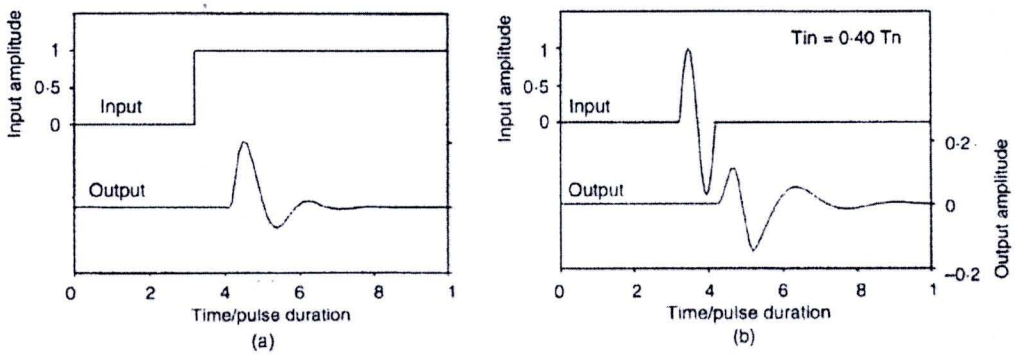

Fig. 2.35 Input pulse of shear wave (a) single square excitation (b) single-shot sinusoidal excitation (Viggiani and Atkinson, 1997)

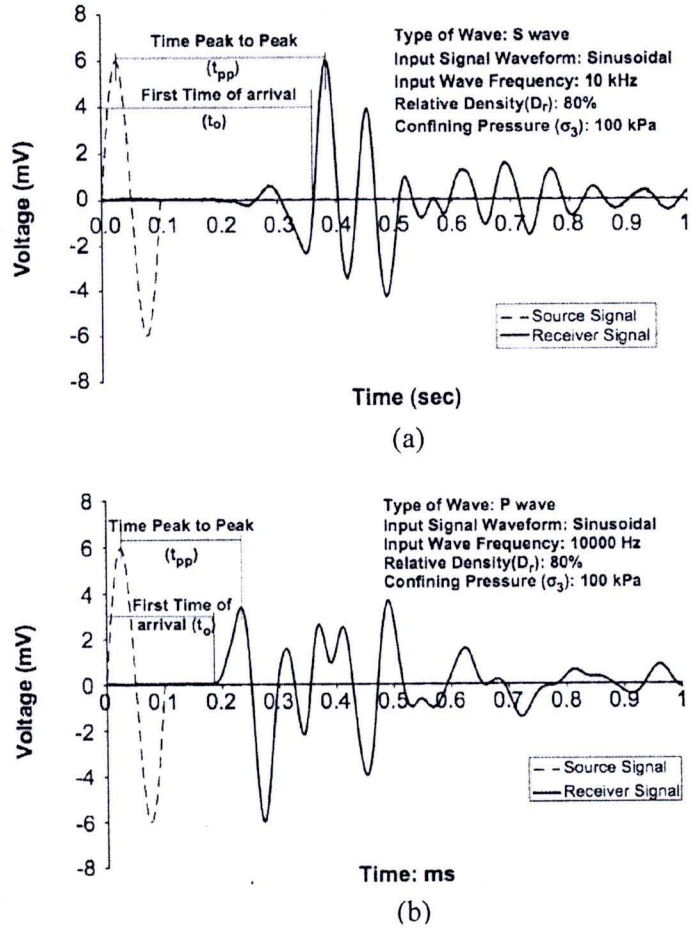

Fig. 2.36 First time of arrival (t_0) and the time between first peak to peak (t_{pp}) with D_r = 80% and σ_3 = 100 kPa (a) with *S-wave* and (a) with *P-wave* (Kumar and Madhusudhan, 2010)

- Travel time between characteristic points

Travel time of shear wave can be taken as the time between two corresponding characteristic points in the single sinusoidal input signal and the output signals. The most commonly used characteristic points are the first peak, first trough, or the zero crossing of the input and output signals. The measurement point, i.e. first peak to peak (t_{pp}), of this technique can be shown in Fig. 2.36a and 2.36b.

- The cross-correlation method

Travel time of the shear wave can be taken as the time shift (t_{cc}) that produces the peak correlation between a single sinusoidal input signal and the output signals. This method is the method which produces the most accurate shear wave velocity results since this method eliminates the ambiguity from visual estimations of other methods. The cross-correlation function $CC_{yx}(t)$ is a measure of the correlation between the receiver signal, $X(t)$ and source signal, $Y(t)$ versus the time shift (τ):

$$CC_{yx}(\tau) = \lim_{\tau \to \infty} \frac{1}{T} \int_{T} X(t)Y(t+\tau)dt \tag{2.8}$$

where T is the total duration of the time record. Typical results with the use of the cross-correlation method are shown in Figs. 2.37a and 2.37b with reference to the propagation of the *S*- and *P-waves*, respectively.

2.3.2.2 Phase-sensitive detection

Blewett *et al.* (1999) explained in their paper that phase-sensitive detection is a standard instrumentation technique. A signal is emitted at a particular frequency. This signal is then combined with noise during its transit to a detector, and then undergoes further degradation before arriving at the final measuring or display device. Even though the signal is now a mixture of many frequencies, the user is usually interested only in that part of the signal at the original emission frequency. A conventional lock-in amplifier can be used just before the final device. This amplifier is fed an electrical copy of the drive signal and derives a reference frequency from it.

The amplifier is also fed the received signal. By multiplication and filtering, the lock-in amplifier extracts information about the strength of the component in the received signal which occurs at the reference frequency. The system can be thought of as a tuneable filter, whose output is usually a direct-current signal proportional to the strength of the reference frequency component within the input signal, as shown in Fig. 2.38.

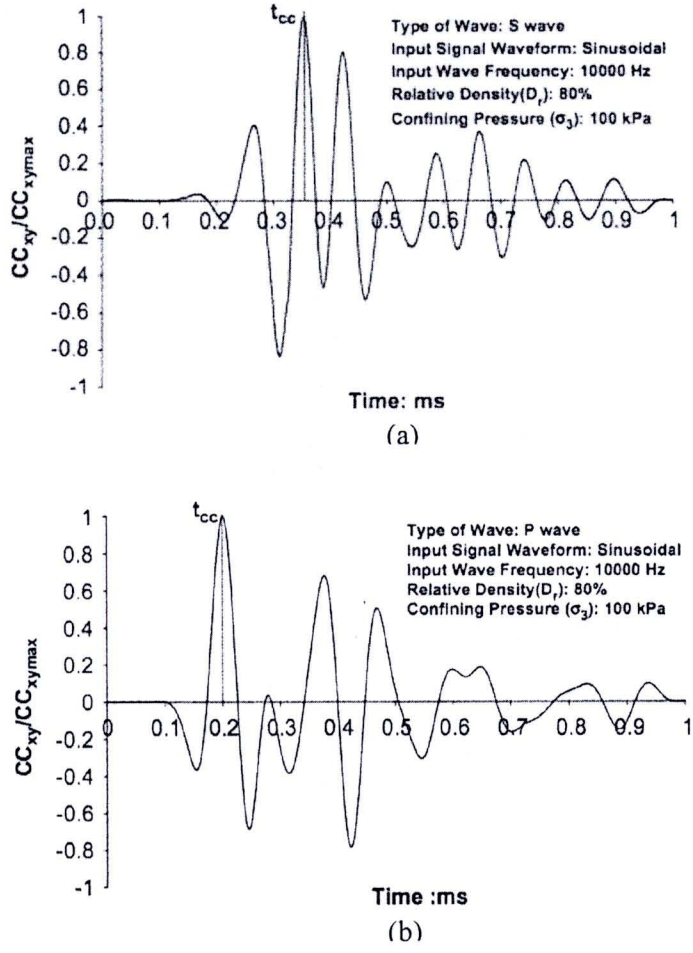

Fig. 2.37 The time of arrival using cross-correlation method (t_{cc}) with D_r = 80%, σ_3 = 100 kPa (a) with *S-wave* and (a) with *P-wave* (Kumar and Madhusudhan, 2010)

The relationship between the change in phase angle and travel time can be determined by:

$$dt = \frac{d\theta}{360f} \tag{2.9}$$

where dt is the change in time-of-flight in seconds, $d\theta$ is the change in phase angle in degrees, and f is the frequency of the driving wave in Hertz.

Depending upon the drive frequency used, small changes in time can result in multiple revolutions of the phase angle and therefore extreme sensitivity.

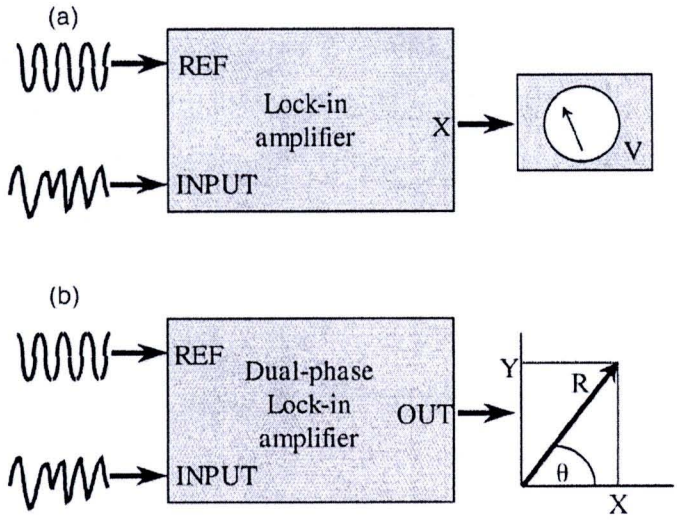

Fig. 2.38 (a) Representation of the lock-in amplifier as a tuneable filter. (b) representation of the output of the dual-phase lock-in amplifier as a vector (Blewett *et al.* 1999)

2.3.3 Potential problems in bender element testing

2.3.3.1 Near-field effect

The travel time of the *S-wave* can be taken as the first arrival of the receiver signal (Leong *et al.* 2005). Reversal of the received signal's polarity when the polarity of the transmitting element is inverted is often taken as the arrival of the *S-wave*. However, numerical studies by some researchers have shown that the first deflection of the S-wave signal may not correspond to the arrival of the *S-wave* but to the arrival of the so-called "near-field" component, which travels with the velocity of the *P-wave*. In addition, inverting the polarity of the transmitter element does not help to eliminate the near-field effect as it produces the reversal of all the waveform components including the near-field components.

Sanchez-Salinero *et al.* (1986) showed that the *S-wave* signal is always accompanied by the propagation of another signal of opposite polarity that travels

with the velocity of the *P-wave*. In other words, the bender element that produces mainly shear displacement will also generate a component that travels at the *P-wave* velocity. This phenomenon is known as the near-field effect, which is quantified in terms of the ratio of wave path length (L_{tt}) to wavelength (λ), L_{tt}/λ. The near-field effect amplitude decays rapidly with increasing number of wavelengths between the transmitter and the receiver element.

Jovicic *et al.* (1996) indicated that the near field effect can be lessen down by increasing the frequency of the input signal. In the literature, most of the bender elements tests have been done at a frequency lesser than 10 kHz. Kumar and Madhusudhan (2010) also concluded that the extent of the near-field effect signal clearly reduces with an increase in the frequency of the input signal. The near-field characteristic of shear wave signal at different frequencies can be displayed in Fig. 2.39.

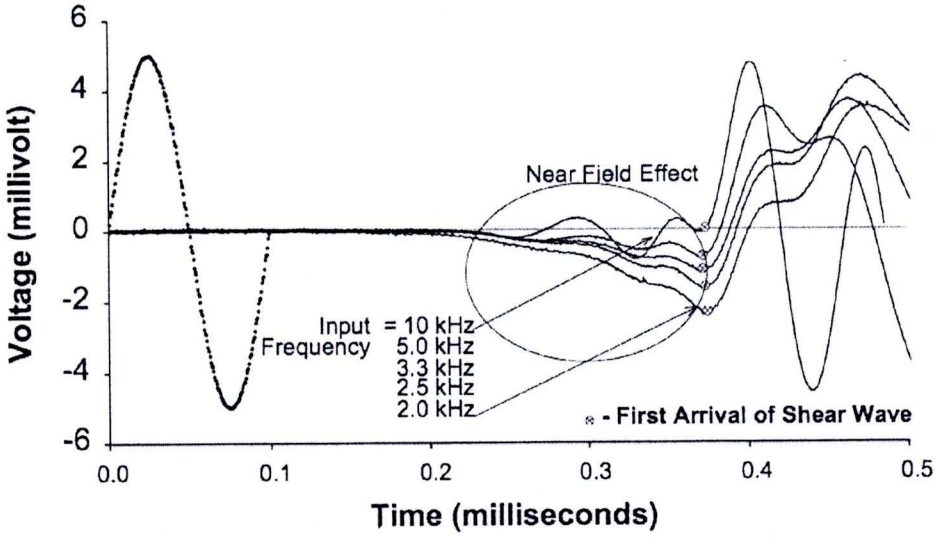

Fig. 2.39 Near-field effect of received shear wave signals at different frequencies (Kumar and Madhusudhan, 2010)

2.3.3.2 Electromagnetic coupling - crosstalk

Lee and Santamarina (2005) explained in their work that electromagnetic coupling between source and receiver bender elements manifests as an output signal with an early component that is quasisimultaneous with the input signal. This

"crosstalk" can be very important in wet soils. Fig. 2.40a shows typical crosstalk effects observed with two series-type bender elements without grounding; the received signal resembles the discharge of a capacitor. Crosstalk can be effectively removed by grounding either the source or the receiver (Fig. 2.40b). The outer electrodes in a parallel-type connection have a shielding effect when connected to ground. Still, crosstalk can be observed in the series-to-parallel combination when the series element is not shielded and grounded (Fig. 2.40c). Crosstalk vanishes when two parallel-type bender elements are used (Fig. 2.40d).

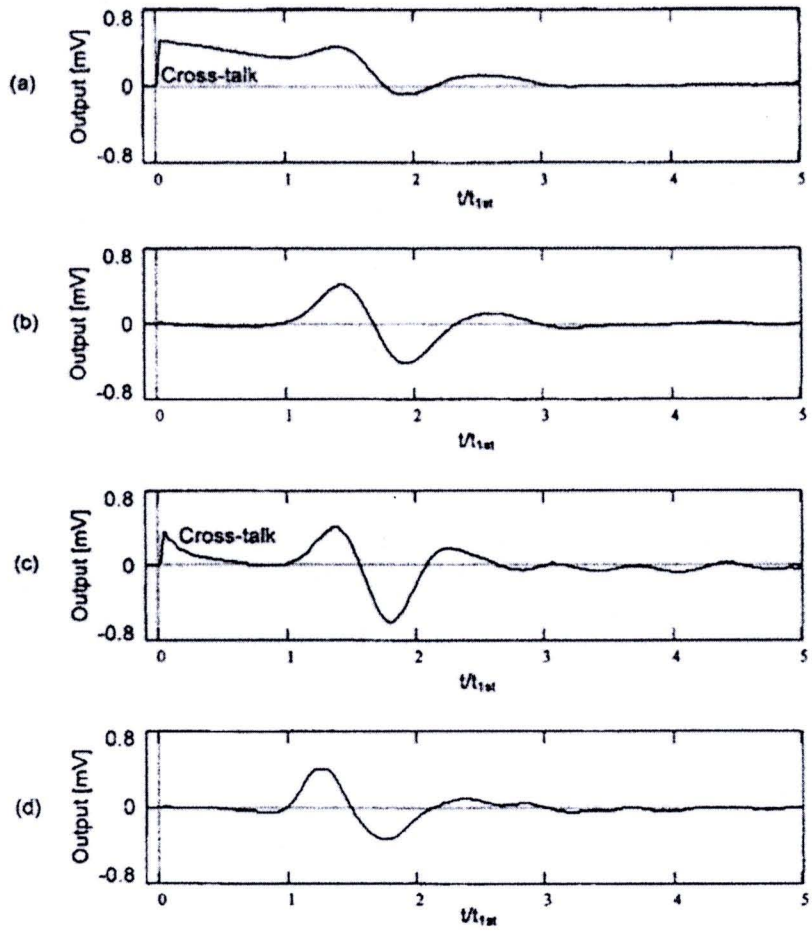

Fig. 2.40 Crosstalk effects: (a) series-to-series without grounding; (b) series-to-series with shielding and grounding; (c) parallel-to-series without shielding and grounding; and (d) parallel-to-parallel without shielding. Time "t_{1st}" corresponds to *S-wave* first arrival (input: step signal, tip-to-tip distance: L = 100 mm) (Lee and Santamarina, 2005)

2.3.3.3 Time or phase lag

The transfer functions relating the physical wave forms to the measured electrical signals introduce significant phase or time lags that are different at the transmitting and receiving benders. The time lag of the system as a whole can be measured by putting bender elements for generating and detecting waves in direct contact with each other. This calibration method was originally proposed by Dyvik and Madshus (1985), who found a nil time lag for small bender transducers. This method was later used by others, e.g. Gajo *et al.* (1997), who found a time lag of 5 μs and 2.8 μs for larger benders.

2.3.3.4 Wave interference and reflection at rigid boundaries

Arulnathan *et al.* (1998) performed bender element tests to investigate how the interference of incident and reflected waves at rigid boundaries can affect the determination of travel time. The transmitter and receiver caps are assumed to be perfectly rigid boundaries and finite elements analyses were done. The results of the finite elements model shows that the correct travel time can be obtained when the ratio of bender separation L to wave length λ is more than or equal to 1/4. In other words the wave length λ must be less than or equal to $4L$, or that there must be at least a quarter wave within the sample separation L. As L/λ decreases below 1/4, travel times are progressively underestimated, and hence shear wave velocity overestimated.